Scientific Reports

https://doi.org/10.1038/s41598-026-38192-5

Article in Press

Integrated metabolomics and 16S rRNA sequencing reveal the mechanism of total flavones of *Abelmoschus manihot* (L.) Medic against liver fibrosis

Received: 2 June 2025

Accepted: 29 January 2026

Published online: 05 February 2026

Cite this article as: Li D., Ge H., Zhang Y. *et al.* Integrated metabolomics and 16S rRNA sequencing reveal the mechanism of total flavones of *Abelmoschus manihot* (L.) Medic against liver fibrosis. *Sci Rep* (2026). https://doi.org/10.1038/s41598-026-38192-5

Dengya Li, Haitao Ge, Yan Zhang, Shuying Song, Luwan Xing, Emily Heya Tang & Fujiang Wang

TITLE PAGE

Integrated metabolomics and 16S rRNA sequencing reveal the mechanism of total flavones of *Abelmoschus manihot* (L.) Medic against liver fibrosis

Dengya Li[a,b], Haitao Ge[a,c], Yan Zhang[c], Shuying Song[c], Luwan Xing[b], Emily Heya Tang[d], Fujiang Wang[a*]

[a] Department of Clinical Medicine and Pharmacology, Jiangsu Suzhong Pharmaceutical R&D Institute Co., Ltd. Nanjing, China

[b] School of Basic Medicine and Clinical Pharmacy, China Pharmaceutical University, Nanjing, China

[c]College of pharmacy, Nanjing University of Chinese Medicine, Nanjing, China

[d] Basis International School Nanjing, Nanjing, China

*** Corresponding author:**

Fujiang Wang

Jiangsu Suzhong Pharmaceutical R&D Institute Co., Ltd. Nanjing, Jiangsu, China

Tel: +86-18351834272

E-mail: wangfj@suzhongyy.com

Author E-mail addresses: 2676455534@qq.com, geht@suzhongyy.com, 2332845032@qq.com, 1501214345@qq.com, 1519847109@qq.com, chenming1622@126.com, wangfj@suzhongyy.com.

Integrated metabolomics and 16S rRNA sequencing reveal the mechanism of total flavones of *Abelmoschus manihot* (L.) Medic against liver fibrosis

Abstract:

Background and aims: To investigate the therapeutic effect of total flavones of *Abelmoschus manihot* (L.) Medic (TFA) on CCl_4-induced liver fibrosis in mice, and to clarify the mechanism of action of TFA in ameliorating liver fibrosis by untargeted metabolomics and intestinal microbiota 16S rRNA sequencing, in order to provide an experimental basis for the clinical application of TFA in the treatment of liver fibrosis.

Methods: To establish a mice model of CCl_4-induced liver fibrosis, and liver injury was assessed through histopathology, liver function markers (ALT, AST), inflammatory cytokines, and oxidative stress indicators. Serum untargeted metabolomics was conducted via LC-MS/MS, and intestinal microbiota profiles were analyzed by 16S rRNA sequencing.

Results: TFA treatment significantly reduced ALT and AST levels by approximately 55% and 40%, respectively, and markedly ameliorated histopathological changes. It also attenuated oxidative stress and inflammation. Metabolomic analysis identified 83

differential metabolites, indicating that TFA restored disruptions in glycerophospholipid, tryptophan, and arachidonic acid metabolism. Gut microbiota sequencing showed that TFA increased beneficial bacteria and decreased harmful bacteria. Furthermore, TFA downregulated the expression of CYP1A1, CYP2E1, and ALOX15 in liver tissue, suggesting modulation of arachidonic acid metabolism.

Conclusion: TFA alleviated CCl_4-induced liver fibrosis in mice by reducing oxidative stress and inflammation, improving gut microbiota dysbiosis, and regulating host metabolism. These findings suggest that TFA may hold potential as a multi-target agent for liver fibrosis, although further studies are required to confirm its efficacy in other models and females.

Keywords total flavones of *Abelmoschus manihot* (L.) Medic, liver fibrosis, serum metabolomics, gut microbiota

1. Introduction

According to the World Health Organization, approximately 844 million people worldwide suffer from chronic liver disease, among which liver fibrosis is a major cause of liver-related mortality. Liver fibrosis is a process in which multiple pathogenic factors persistently stimulate liver tissue, resulting in diffuse overdeposition and abnormal distribution of hepatic extracellular

matrix[1, 2]. Liver fibrosis is the pathological repair response of the liver to chronic injury, and it is a key step in the progression of various chronic liver diseases to cirrhosis[3, 4]. Studies have shown that attenuating or eliminating multiple causative factors of liver fibrosis can reverse it to some extent. Therefore, early intervention in the treatment of liver fibrosis is important in reducing the incidence of severe liver disease[5]. However, there is still a lack of potent anti-liver fibrosis drugs in clinical practice, and the development of anti-liver fibrosis drugs, especially the search for active ingredients with multi-target effects from natural plants, has become one of the hotspots in current research.

Traditional Chinese medicine, with its high efficiency and low toxicity, has shown good results in the treatment of liver fibrosis. Abelmoschi corolla is the dried corolla of *Abelmoschus manihot* (L.) Medic (AM). Modern pharmacological research have shown that it has anti-inflammatory, antibacterial, and antioxidant activities[6], and it is widely used in the treatment of inflammatory diseases. Huangkui capsule (HKC) developed by Suzhong Pharmaceutical Group Co., Ltd. is an extract preparation of the AM, which has been approved by the State Food and Drug Administration of China (Z19990040) for the treatment of chronic kidney disease[7]. Studies have shown that the total flavones of *Abelmoschus manihot*

(TFA) are the main components of it. Our group previously characterized the seven flavone glycosides in TFA by high-performance liquid chromatography (HPLC). The total flavonoid content was determined using the one-measurement-multiple-assessment method, and the content calculation was performed by the relative correction factor of each flavonoid using hyperoside as the internal standard. The TFA profile composition was the following: 43.2% hyperoside, 27.1% hibifolin, 13.7% isoquercetin, 8.8% quercetin3'-O-glucoside, 3.8% quercetin-3-O-robinobioside, 3.2% myricetin and 0.2% quercetin[8, 9].

Studies have reported that flavonoid constituents have anti-liver fibrosis effects and their mechanisms of action are related to anti-inflammatory, anti-oxidative stress, anti-apoptotic, and inhibition of abnormal accumulation of extracellular matrix. Previous studies indicated that TFA exerts protective effects against acute liver injury and cholestasis through anti-inflammatory and antioxidant mechanisms[10]. However, most prior research focused on acute or cholestatic injury models, and the anti-fibrotic mechanisms of TFA, particularly concerning chronic liver fibrosis, remain poorly elucidated. Specifically, the potential modulation of arachidonic acid metabolism and gut-liver axis interactions has not

been systematically investigated.

The pathogenesis of liver fibrosis is complex, in addition to inflammation-induced, changes in intestinal microbiota and abnormalities in body metabolism may also induce or exacerbate liver injury[11, 12]. As an important immune organ in the human body, intestinal microbiota maintains a dynamic balance with its internal and external environment and participates in the body's immune, nutritional and metabolic functions[13, 14]. Dysregulation of intestinal microbiota is considered to be an important pathological feature of certain metabolic system diseases, especially chronic liver diseases[15]. Metabolomics, with its advantages of “systematic, time-sequential and comprehensive”, is highly compatible with the multi-component, multi-pathway and multi-target mode of action of traditional Chinese medicines, and has become an important research tool for revealing the mechanism of action of traditional Chinese medicines[16-18]. The combined analysis of intestinal microbiota and metabolomics provides insight into the correlations between microbial communities and metabolites in organisms to reveal their functions and interactions in organismal health and disease[19, 20].

In contrast to earlier reports on acute or cholestatic liver injury models, this study focuses specifically on CCl_4-induced chronic liver

fibrosis. We employed an integrated approach combining untargeted serum metabolomics (LC-MS/MS) and 16S rRNA sequencing of intestinal microbiota to comprehensively investigate the anti-liver fibrosis mechanisms of TFA. Our research aims to identify key metabolic pathways and microbial communities influenced by TFA, with particular emphasis on arachidonic acid metabolism and gut-liver interactions. We further validated critical targets within the arachidonic acid metabolic pathway to clarify the mechanistic basis of TFA's protective effects. This study provides a novel, systems-level understanding of TFA against liver fibrosis and offers new insights for clinical applications and traditional Chinese medicine research.

2. Materials and methods

2.1 Reagents and materials

TFA was obtained from Suzhong Pharmaceutical Group Co., Ltd. (Taizhou, China). Carbon tetrachloride (CCl_4) and colchicine were purchased from Macklin Chemical Technology Co., Ltd. (Shanghai, China). Olive oil was purchased from Shanghai Titan Scientific Co., Ltd. (Shanghai, China). Mouse ELISA detecting kits were purchased from Jiangsu Meimian Industrial Co., Ltd (Meimian, Jiangsu, China). CYP1A1 (apcepta, Suzhou, China, Cat#Ap7993B), CYP2E1 (HUABIO, Hangzhou, China, Cat#ET1703-48), ALOX15

(apcepta, Suzhou, China, Cat#AP7896B).

2.2 Animals

60 male C57BL/6J mice (18-22 g) were obtained from the Sbf (Suzhou) Biotechnology Co., Ltd.[License No.: SCXK (SU) 2022–0006]. The mice were kept in a controlled environment (24±1℃ and 40%-60% humidity) with free access to tap water and food under a 12 h light/dark cycle. Our study was performed in accordance with the guidelines of National Institutes of Health for the human use of animals. All animal experiments were approved by the Animal Ethics Committee of Suzhong Pharmaceutical Group Co., Ltd. (Approval Code: SZSW-2023082401).

2.3 Modeling and interventions

The mice were acclimatized and fed for one week, and then were randomly divided into the control group, model group, colchicine group, TFA low-dose group (TFA-L), TFA medium-dose group (TFA-M), and TFA high dose group (TFA-H) (n=10). The control group was only intraperitoneally injected with olive oil and the other five groups were i.p. injected with a mixture of CCl_4 and olive oil [1:9 (v/v)] (5 mL/kg body weight) twice a week for 6 weeks to induce liver fibrosis[21]. Then TFA (39, 78, 156 mg/kg/day) and colchicine (0.1 mg/kg/day, as a positive control group) were

administered with vehicle by oral gavage for 4 weeks, except for the control and model groups.

The TFA dosage was calculated based on the clinical dosage of HKC. According to our in-house quantitative analysis, the TFA content in HKC accounts for approximately 8% of the total capsule weight. Based on the clinical dosage of HKC, which is 0.6 g/day for adults, we calculated the equivalent dose of TFA for mice to be 78 mg/kg/day using the standard body surface area conversion method. Then, the low, medium, high doses set as 0.5×, 1×, 2× the clinical equivalent to assess dose-response relationships.

2.4 Sample collection

At the end of the experiment, all animals were fasted and given isoflurane inhalation anesthesia for samples collection. Terminal blood samples were collected aseptically from the retro-orbital venous plexus using glass capillary tubes. The samples were placed in blank tubes without anticoagulant, allowed to clot at room temperature for 30 minutes, and then centrifuged at 3500 rpm for 15 minutes to obtain serum. Serum were stored at -80℃ for the biochemical parameters and metabolomics analysis.

After blood samples were collected, mice were euthanized by cervical dislocation, and livers were immediately collected,

weighed and recorded. A portion of the left lobe of the liver was fixed in 10% neutral-buffered formalin for the histopathological and immunohistochemical examinations. The remaining liver tissue was rinsed with pre-cooled saline, dried on filter paper, quick-frozen in liquid nitrogen and transferred to -80°C refrigerator for storage.

Then the entire intestines were dissected with a sterile scalpel, and the contents of the intestines were collected with sterile lyophilized tubes (100-200 mg/tube). Fresh intestinal contents from each group were immediately frozen in a liquid nitrogen tank and then stored at −80℃ for the 16S rRNA sequencing analysis.

2.5 Histopathological analysis

The 10% neutral-buffered formalin-impregnated liver tissue was dehydrated, embedded in paraffin, sectioned, stained with HE staining, Masson staining and sealed with neutral resin. The tissue sections were scanned with a tissue section scanner to observe the damage of hepatocytes, inflammatory cell infiltration and collagen deposition.

2.6 Untargeted serum metabolomics LC-MS/MS assay

Metabolites Extraction

The serum samples (100 μL) were placed in the Eppendorf (EP) tubes and resuspended with prechilled 80% methanol by well vortex. Then the samples were incubated on ice for 5 min and

centrifuged at 15000 g, 4°C for 20 min. Some of supernatant was diluted to final concentration containing 53% methanol by LC-MS grade water. The samples were subsequently transferred to a fresh EP tube and then were centrifuged at 15000 g, 4°C for 20 min. Finally, the supernatant was injected into the LC-MS/MS system analysis[22, 23].

UHPLC-MS/MS Analysis

UHPLC-MS/MS analyses were performed using a Vanquish UHPLC system (ThermoFisher, Germany) coupled with an Orbitrap Q ExactiveTMHF-X mass spectrometer (ThermoFisher, Germany).

Samples were injected onto a HypersilGoldcolumn (100×2.1 mm, 1.9 μm) using a 17-min linear gradient at a flow rate of 0.2mL/min. The eluents for the positive polarity mode were eluent A (0.1%FA in Water) and eluent B (Methanol).The eluents for the negative polarity mode were eluent A (5 mM ammonium acetate, pH 9.0) and eluent B (Methanol).The solvent gradient was set as Table 1.

Q ExactiveTM HF mass spectrometer was operated in positive/negative polarity mode with spray voltage of 3.5 kV, capillary temperature of 320°C, sheath gas flow rate of 35 psi and aux gas flow rate of 10 L/min, S-lens RF level of 60, Aux gas heater temperature of 350°C.

Data processing and metabolite identification

The raw data files generated by UHPLC-MS/MS were processed using the Compound Discoverer 3.3 (CD3.3, ThermoFisher) to perform peak alignment, peak picking, and quantitation for each metabolite. The main parameterswere set as follows: peak area was corrected with the first QC; actual mass tolerance, 5ppm; signal intensity tolerance, 30%; and minimum intensity, et al. After that, peak intensities were normalized to the total spectral intensity. The normalized data was used to predict the molecular formula based on additive ions, molecular ion peaks and fragment ions. And then peaks were matched with the mzCloud (https://www.mzcloud.org/), mzVaultand MassListdatabase to obtain the accuratequalitative and relative quantitative results. Statistical analyses were performed using the statistical software R (R version R-3.4.3), Python (Python 2.7.6 version) and CentOS (CentOS release 6.6), When data were not normally distributed, standardize according to the formula: sample raw quantitation value / (The sum of sample metabolite quantitation value / The sum of QC1 sample metabolite quantitation value) to obtain relative peak areas; And compounds whose CVs of relative peak areas in QC samples were greater than 30% were removed, and finally the

metabolites' identification and relative quantification results were obtained.

Data Analysis

The preprocessed data were imported into SIMCA-P software for principal component analysis (PCA) and orthogonal partial least squares discriminant analysis (OPLS-DA) to screen for differential metabolites with VIP>1 and $P<0.05$. The identified differential metabolites were annotated using KEGG database and HMDB database[24, 25]. Serum differential metabolites in positive and negative ion patterns were combined. Differential metabolic pathway analysis was performed on the differential metabolites by MetaboAnalyst 6.0.

Table 1. Gradient conditions.

Time (min)	A%	B%
0	98	2
1.5	98	2
3	15	85
10	0	100
10.1	98	2
11	98	2
12	98	2

2.7 16S rRNA sequencing and Bioinformatics *analysis*

Total genome DNA from samples was extracted using CTAB method. DNA concentration and purity was monitored on 1% agarose gels. According to the concentration, DNA was diluted to

1ng/μL using sterile water. 16S rRNA genes of distinct regions (16S V4) were amplified used specific primer (515F(5’-GTGCCAGCMGCCGCGGTAA-3’) and 806R (5’-GGACTACHVGGGTWTCTAAT-3’)) with the barcode. The PCR amplification products were purified, quantified and normalized to form sequencing libraries, which were up-sequenced using the Illumina sequencing platform.

Paired-end reads from the original DNA fragments were imported, quality-filtered, denoised□merged, and then the chimeric sequences were identified and removed using the QIIME2 dada2 plugin to obtain the feature table of amplicon sequence variant (ASV) [26].

This method provides a higher resolution than traditional OTU clustering by inferring exact biological sequences and removing sequencing errors[27-29]. For clarity and consistency with widespread convention in the literature, the term ‘OTU’ (Operational Taxonomic Unit) is used throughout the text to refer to these feature sequences. Taxonomic assignment of ASVs was performed against the SILVA database (version 138) and the mouse microbial database to obtain species classification information. Subsequent analyses, including taxonomic composition at the phylum to genus levels, as well as Alpha and Beta diversity

analyses, were based on the resulting ASV table.

2.8 Immunohistochemistry analysis

Tissue sections were deparaffinized, rehydrated, and subjected to antigen retrieval. Endogenous peroxidase activity was blocked with 3% H_2O_2, followed by incubation with 5% BSA. Primary antibody was applied overnight at 4℃. After washing, a horseradish peroxidase (HRP)-conjugated secondary antibody was incubated. Signal detection was performed using DAB substrate, followed by hematoxylin counterstaining. Slides were dehydrated, mounted, and imaged under a microscope. Semi-quantitative analysis was performed using ImageJ software.

2.9 Western blotting

Mouse liver tissues were lysed in RIPA lysis buffer (Aidisheng, Jiangsu, China) supplemented with protease inhibitors (Aidisheng, Jiangsu, China). The supernatant was collected after centrifugation at 12,000 r for 15 min at 4°C. Protein concentration was determined using a BCA Protein Assay Kit (Aidisheng, Jiangsu, China). A total of 40 μg of the protein sample was loaded into sodium dodecyl sulfate polyacrylamide gel electrophoresis (SDS-PAGE). After being transferred to the PVDF membrane and blocked with 5% skim milk for 2 h at room temperature, the membrane was incubated with primary antibody and secondary

antibody. The peroxidase activity of bands was detected using the chemiluminescent detection kit (Vazyme, Jiangsu, China). The primary and secondary antibodies used were: CYP1A1 (raised in rabbit, 1:1000; abcepta), CYP2E1 (raised in rabbit, 1:1000; abcepta), ALOX15 (raised in rabbit, 1:1000; abcepta), α-SMA (raised in rabbit, 1:2000; proteintech), collagen III (raised in rabbit, 1:500; proteintech), and β-actin (raised in rabbit, 1:5000; proteintech).

2.10 Statistical analysis

All data are presented as means ± standard deviation (SD). Statistical analyses were performed using GraphPad Prism 8.0 software. For comparisons between two groups, Student's t-test was used. For comparisons among multiple groups, one-way analysis of variance (ANOVA) was performed, followed by Bonferroni's post hoc test. To control the false discovery rate (FDR) in multiple hypothesis testing—such as in metabolomic, microbiota, and correlation analyses—p-values were adjusted using the Benjamini-Hochberg method. Differences with a corrected p-value (FDR) < 0.05 were considered statistically significant.

3. Results

3.1 Protective effect of TFA against CCl_4-induced liver fibrosis in mice

The mice were sacrificed and liver tissues were collected at the end of the experiment, and the apparent characteristics of the mice liver were observed, as shown in Fig. 1A. As shown in Fig. 1B, compared with the control group, the liver index of the model group mice was significantly elevated (P<0.01), and compared with the model group, the liver index of the mice in each dosing group was significantly reduced (P<0.01). As shown in the Fig. 1C-E, ALT, AST and ALP levels were significantly higher in the model group compared with the control group (P<0.01), indicating that repeated stimulation with CCl_4 led to liver injury. Compared with the model group, the levels of ALT, AST, and ALP were significantly reduced in each dosing group (P<0.05, 0.01), suggesting that TFA had a significant improvement effect on the liver function of CCl_4-induced liver fibrosis in mice.

H&E staining and Masson staining were used for histological analysis of the livers. As shown in Fig. 1F, the liver morphology of control mice was normal, in the model group, the fibrous septum segmented the liver confluent area to form pseudolobules, with obvious punctate necrosis of hepatocytes, proliferation of abnormal hepatocytes and edema and inflammatory cell infiltration. Compared with the model group, administration of colchicine and TFA in each dose group significantly improved hepatocellular

necrosis and inflammatory cell infiltration, and pseudolobules became significantly less frequent. Masson staining results as shown in Fig. 1G, the control group mice liver tissue lobules, confluence area and central vein around only see less collagen fibers, the model group can be seen a large number of blue collagen fibers, colchicine and TFA can be different degrees to reduce the area of collagen fibers in the liver tissue.

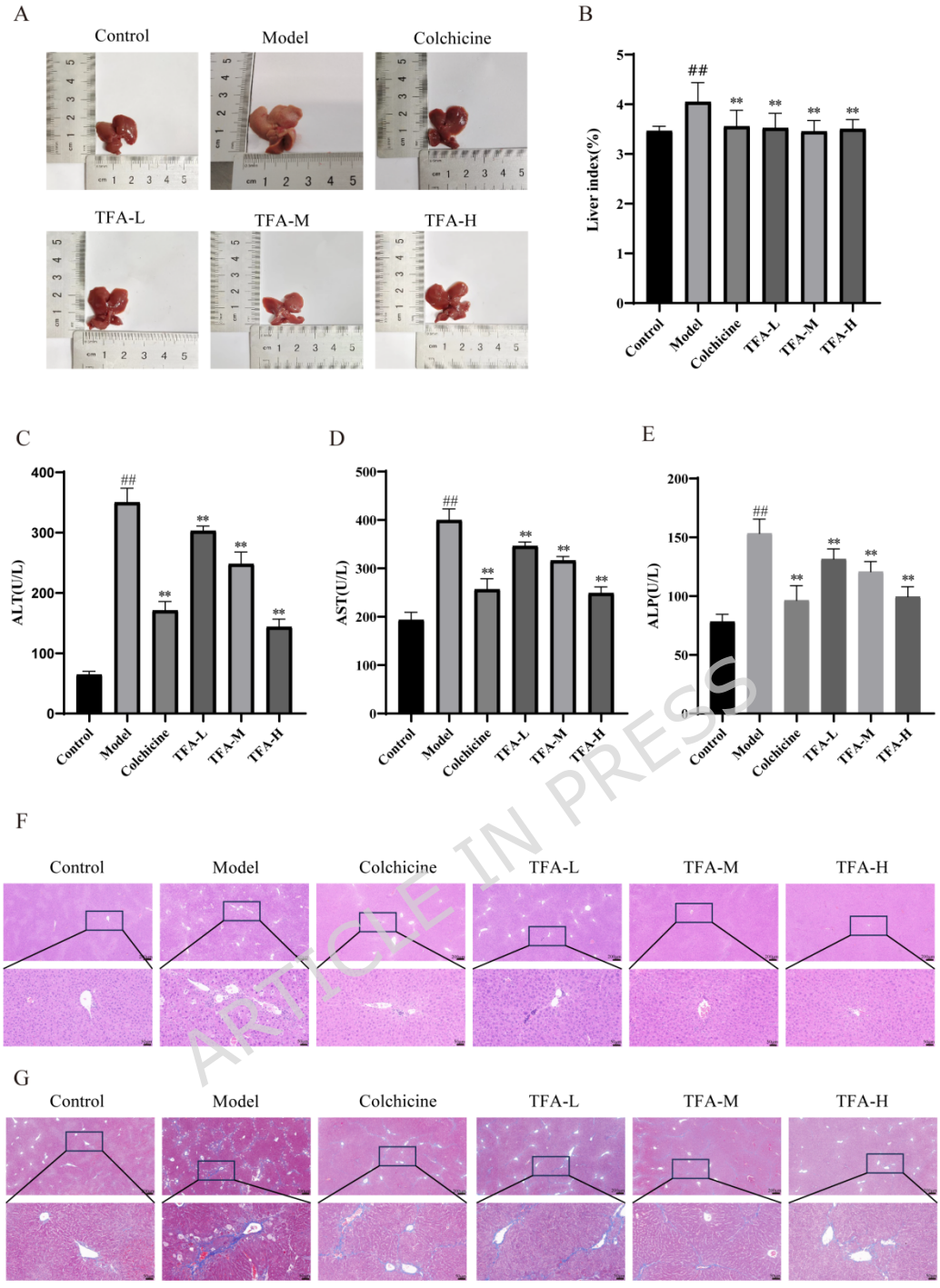

Fig.1. Effect of TFA on liver function and histopathology of liver fibrosis. (A) Representative liver maps of each group.(B) Liver index of mice. (C) TFA decreased serum ALT level. (D) TFA decreased serum AST level. (E) TFA decreased serum ALP level. (F) Representative H&E-stained sections of liver tissue. (G) Representative Masson-stained sections of liver tissue. 50×, bar=200 μm; 200×, bar=50 μm. Data were expressed as mean ± SD (n=10). $^{\#}P<0.05$, $^{\#\#}P< 0.01$, vs control group. $^{*}P<0.05$, $^{**}P<0.01$, vs model group.

3.2 TFA attenuates oxidative stress and inflammatory response and ameliorates liver fibrosis in mice

As shown in Fig. 2A-C, compared with the control group, the SOD and GSH-Px levels of mice in the model group were significantly reduced (P<0.01), and the MDA level was significantly increased(P<0.01). Compared with the model group, SOD activity was significantly higher in the colchicine group and the medium and high dose groups of TFA (P<0.05), GSH-Px level was significantly higher in the mice of each dosing group (P<0.05), and MDA level was significantly lower (P<0.01).

As shown in the Fig. 2D-F, compared with the control group, the serum TNF-α, IL-6 and TGF-β1 levels of mice were significantly higher in the model group (P<0.01). Compared with the model group, the serum TNF-α level of mice in the colchicine group and the TFA-H group was significantly lower (P<0.01), the IL-6 level in the colchicine group and the medium and high dose groups of TFA was significantly lower (P<0.05, 0.01), and the TGF-β1 level in the respective dosing groups was significantly lower (P<0.05, 0.01).

As shown in the Fig.2G, compared with the control group, the hepatic tissue Hydroxyproline (HYP) content of mice in the model group was significantly higher (P<0.01); compared with the model group, the hepatic tissue HYP content of mice in the colchicine

group and the medium and high dose groups of TFA was significantly lower (P<0.05, 0.01).

As shown in the Fig. 2H-I, compared with the control group, the serum levels of Collagen IV (Col-Ⅳ) and Hualuronic acid (HA) were significantly increased in the model group (P<0.01). Compared with the model group, the serum Col-Ⅳ level of mice in each dosing group was significantly decreased (P<0.05, 0.01), and the HA level of mice in the colchicine group and the medium and high dose groups of TFA was significantly decreased (P<0.05, 0.01).

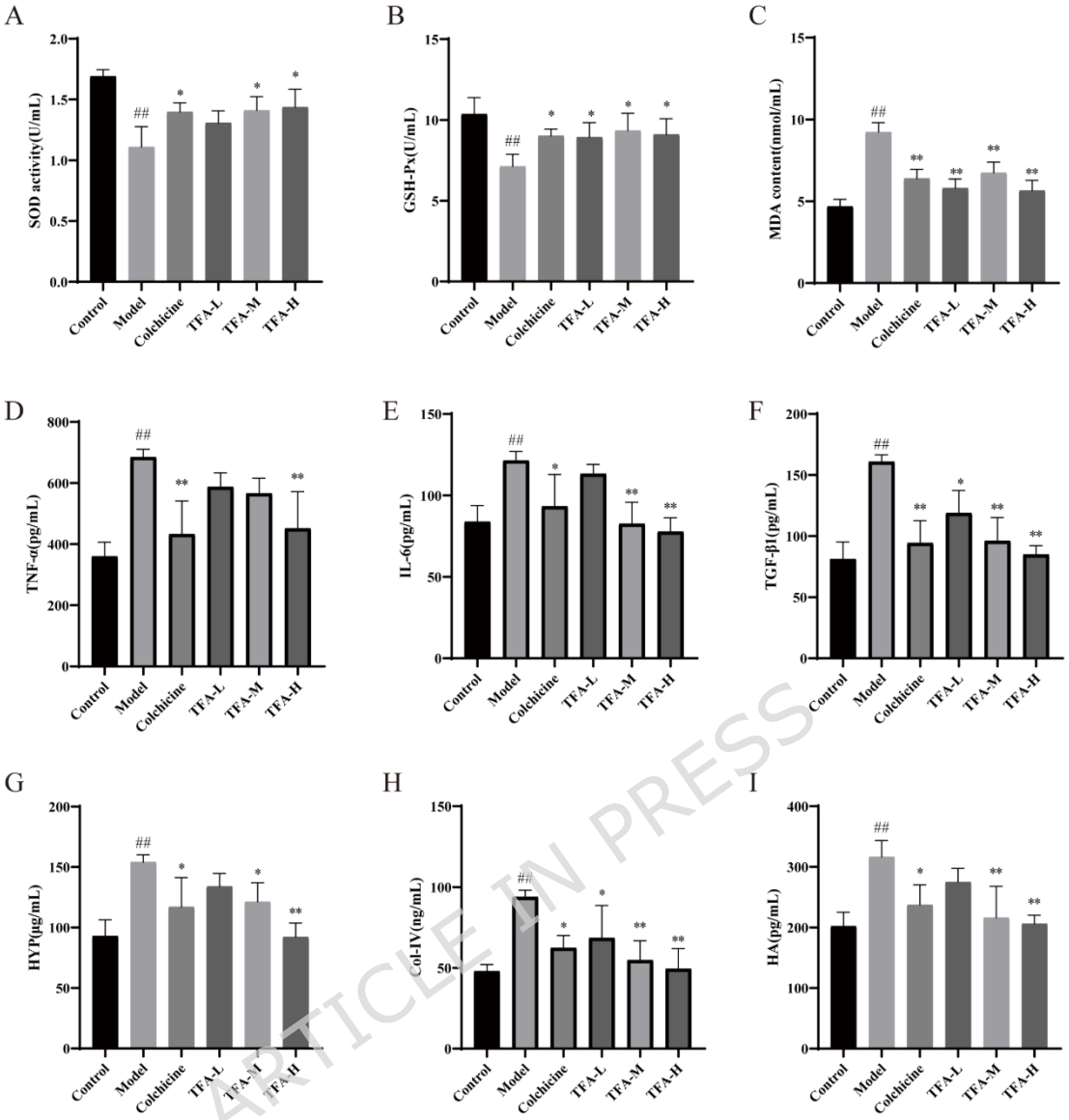

Fig.2. TFA alleviated oxidative stress and inflammatory response expression during liver fibrosis. (A-C) The expression levels of indicators of oxidative stress SOD, GSH-Px and MDA in each group. (D-F) The expression levels of inflammatory factors TNF-α, IL-6 and TGF-β1 in each group. (G-I) The expression levels of HYP, Col-Ⅳ and HA in each group. Data were expressed as mean±SD (n=10). $^{\#}P<0.05$, $^{\#\#}P<0.01$, vs control group. $^{*}P<0.05$, $^{**}P<0.01$, vs model group.

3.3 Differential metabolite and metabolic pathway analysis

To investigate the metabolic differences among the control,

model and TFA-H groups, PCA and OPLS-DA multivariate statistical analyses were performed on the serum metabolomics data of mice. The PCA score plots (Fig. 3A-B) showed that the metabolic compositions of samples from the three groups showed a tendency to segregate, and a significant segregation occurred in particular for the control group and the model group, suggesting that CCl_4 caused differences in the serum metabolites of mice. To further clarify the differences in metabolites, OPLS-DA was used to further analyze the serum samples of mice, and the separation between the control group and the model group was obvious and the degree of aggregation was better in the OPLS-DA score plots (Fig. 3C, E). In order to test whether the OPLS-DA model had overfitting phenomenon, the OPLS-DA model was statistically validated by the replacement test (Fig. 3D, F), the positive ion mode (R^2Y=0.975, Q^2=0.836) and the negative ion mode (R^2Y=0.98, Q^2=0.874). The closer the R^2Y and Q^2 are to 1, it means that the model is more effective in distinguishing the difference.

Differential analysis of all detected metabolites was performed based on OPLS-DA, and metabolite volcano maps were drawn to observe the distribution of differential metabolism. Compared with the control group, CCl_4 induced dramatic changes in metabolites, in which 300 metabolites were up-regulated and 200 metabolites

were down-regulated (Fig. 3G). Whereas, high-dose TFA increased the levels of 313 metabolites and decreased 227 metabolites (Fig. 3H).

Based on the OPLS-DA model, VIP>1 and P<0.05 were used as the critical indicators to identify differentially expressed metabolites. A total of 317 differentially expressed metabolites were identified, and 83 metabolites (50 metabolites in positive ion mode and 33 metabolites in negative ion mode) were identified based on the HMDB and KEGG database. Detailed information is presented in Table S1.

To prioritize the most relevant metabolites for biological interpretation, we focused on those with the highest VIP scores and most significant p-values. Table S2 summarizes the top 8 ranked differentially expressed metabolites between the Model and Control groups, along with their biological implications related to liver pathology. Key altered metabolites included: 20-HETE and 16(R)-HETE: These hydroxyeicosatetraenoic acids, metabolites of arachidonic acid, were significantly upregulated in model mice. 20-HETE is a potent pro-inflammatory and vasoactive lipid mediator known to promote oxidative stress and activate pro-fibrotic signaling pathways[30]. Phenylpyruvic acid: The downregulation of this phenylalanine metabolite suggests a

potential disruption in amino acid metabolism and energy homeostasis, often associated with liver dysfunction. Phosphocholine: As a key precursor in glycerophospholipid metabolism, its decreased level indicates a disturbance in membrane phospholipid synthesis and possibly impaired hepatic secretion of very-low-density lipoproteins (VLDL)[31, 32]. The trends of these top-ranked metabolites were significantly reversed by TFA intervention (Fig. 4), underscoring their relevance to the therapeutic effect of TFA.

Subsequent metabolic pathway analysis of the 83 metabolites was performed using MetaboAnalyst 6.0. Thirteen pathways were initially identified based on a pathway impact value>0.1 (Fig. 3I). Detailed information is shown in Table 2. However, after FDR correction, only glycerophospholipid metabolism (FDR=0.50), tryptophan metabolism (FDR=0.50), and biotin metabolism (FDR=0.50) showed relatively stronger statistical support among those with higher topological impact, although none reached a conventional FDR significance threshold (FDR<0.05).

Notably, arachidonic acid metabolism, despite a higher pathway impact value (0.35), exhibited a less significant p-value (0.13) and high FDR (0.79), suggesting its potential biological relevance may require further validation. Other pathways,

including phenylalanine metabolism, steroid hormone biosynthesis, caffeine metabolism, and histidine metabolism, showed FDR values equal to 1, indicating limited statistical confidence after multiple testing correction.

Therefore, subsequent biological interpretation focuses primarily on glycerophospholipid metabolism, tryptophan metabolism, biotin metabolism, and—given its high mechanistic relevance—arachidonic acid metabolism.

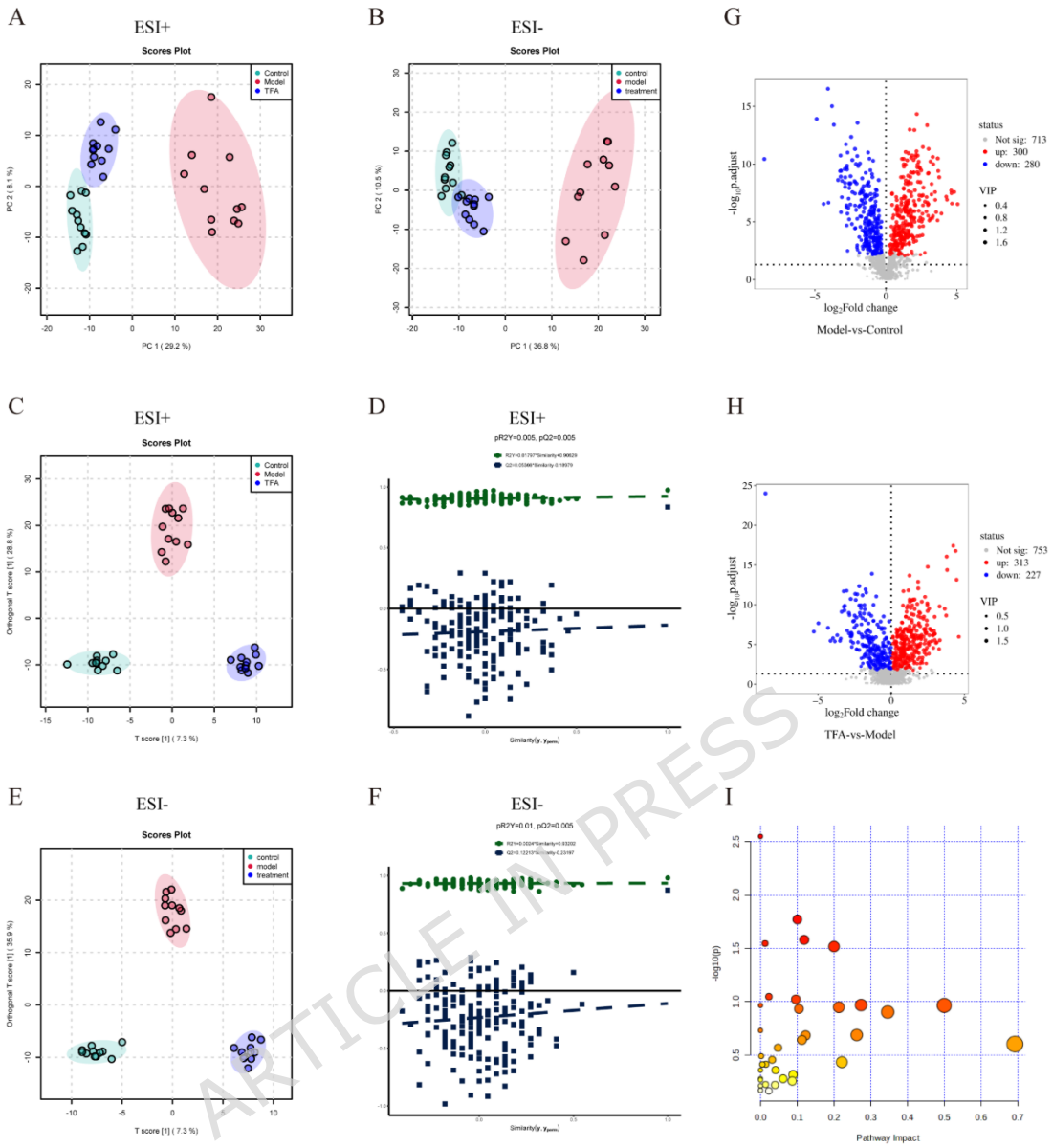

Fig.3. TFA regulates metabolomics in serum of CCl_4-induced liver fibrosis mice. (A-B) PCA plot of metabolites in serum under positive and negative ion modes. The ellipse represents the 95% confidence interval. (C-D) OPLS-DA score chart and 200-permutation test results under positive ion modes (R^2Y=0.975, Q^2=0.836) .(E-F) OPLS-DA score chart and 200-permutation test results under negative ion modes (R^2Y=0.98, Q^2=0.874). (G-H) Volcano plots showing differentially expressed metabolites. Red dots represent up-regulated metabolites, blue dots represent down-regulated metabolites, and grey dots

represent not-significant changes ($|\log_2 FC| > 1$, p.adjust<0.05). (I) Metabolic pathways of differential metabolites[24].

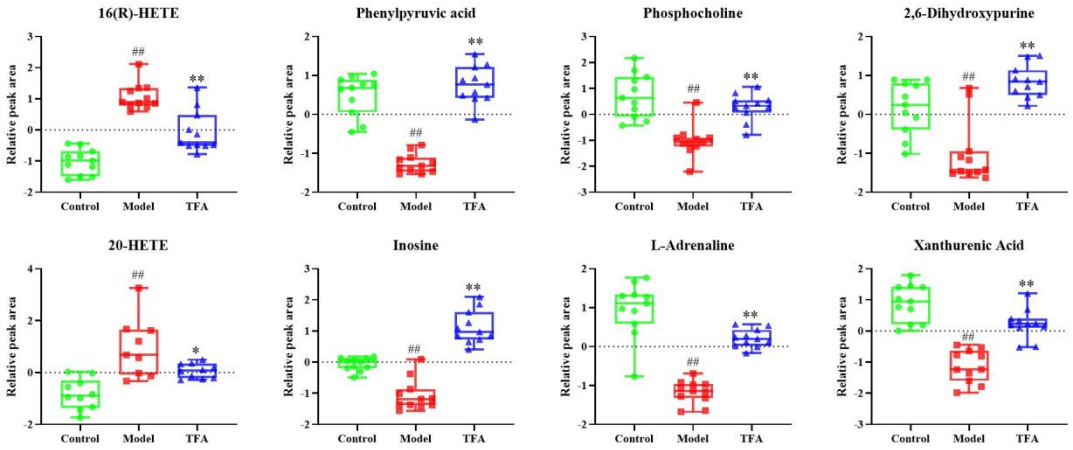

Fig.4. Key differential metabolites profiles. Box plots show relative levels of representative metabolites in the Control (green), Model (red), and TFA-H (blue) groups. Data were expressed as mean±SD (n=10). ## indicates FDR-adjusted p < 0.01 vs. Control; # indicates FDR-adjusted p < 0.05 vs. Control; ** indicates FDR-adjusted p < 0.01 vs. Model.

Table 2. Results of metabolic pathways with MetaboAnalyst 6.0.

Pathway Name	Total	Hits	P value	-log(p)	FDR	Impact
Glycerophospholipid metabolism	36	4	0.01757	1.7552	0.49686	0.10069
Tryptophan metabolism	41	4	0.027228	1.565	0.49686	0.11883
Biotin metabolism	10	2	0.031054	1.5079	0.49686	0.2
Fructose and mannose metabolism	20	2	0.10958	0.96028	0.78884	0.27363
Riboflavin metabolism	4	1	0.10958	0.96027	0.78884	0.5
Amino sugar and nucleotide sugar metabolism	42	3	0.11551	0.93738	0.78884	0.21306
beta-Alanine metabolism	21	2	0.11898	0.92452	0.78884	0.10448
Arachidonic acid metabolism	44	3	0.12819	0.89216	0.78884	0.34609
Phenylalanine metabolism	8	1	0.20739	0.68321	1	0.2619
Lysine degradation	30	2	0.21047	0.67681	1	0.1227
Steroid hormone biosynthesis	87	4	0.23433	0.63018	1	0.11256
Caffeine metabolism	10	1	0.25227	0.59813	1	0.69231
Histidine metabolism	16	1	0.37253	0.42884	1	0.22131

3.4 Effect of TFA on the intestinal microbiota of mice with liver fibrosis

The 16S rRNA genes in the intestine contents from CCl_4-induced liver fibrosis mice were sequenced and analyzed. Species diversity of each group of intestinal microbiota was assessed by alpha diversity analysis. As shown in Fig. 5A-C, compared with the control group, the Chao 1 index, Shannon index and Simpson index of the model group decreased significantly (P<0.05, 0.01); compared with the model group, the Chao 1 index, Shannon index and Simpson index of the TFA group increased significantly (P<0.05, 0.01). This suggests that TFA may influence the structural changes of intestinal microbiota in CCl_4-induced liver fibrosis mice by changing the relative abundance and community diversity of the microbiota.

β-diversity was to analyze the species differentiation between samples, and principalco-ordinatesanalysis (PCoA) and non-metric multidimensional scaling analysis (NMDS) are usually used to study the composition of the intestinal microbiota between groups. PCoA and NMDS analyses showed that (Fig. 5D, E), there was a significant difference in the composition of the intestinal microbiota of mice in the control and model groups; the difference in the intestinal microbiota of mice after TFA treatment was obvious and

its distribution tended to migrate towards the control group, suggesting that TFA had a certain regulatory effect on the composition of the intestinal microbial community in mice with liver fibrosis.

The intergroup microbiota variability at the phylum and genus level was analyzed. At the phylum level, as shown in Fig. 5F, compared with the control group, the abundance of *Firmicutes* and *Actinobacteriota* significantly decreased , the abundance of *Proteobacteria* and *Bacteroidetes* increased in the model group. Compared with the model group, the abundance of *Firmicutes* and *Actinobacteriota* significantly increased, the abundance of *Proteobacteria* and *Bacteroidetes* decreased in the TFA group. At the genus level, as shown in Fig. 5G, compared with the control group, the abundance of *Stenotrophomonas_A_615274*, *Comamonas_F_589250*, *Dwaynesavagella*, and *Chryseobacterium_796614* increased, while the abundance of *Dubosiella*, *Lactobacillus*, *Ligilactobacillus*, *Desulfovibrio_R_446353*, *Bifidobacterium_388775* decreased in the model group. The intervention of TFA corrected the changes in the above genera compared to the model group.

LEfSe analysis was used to analyze differential species at multiple levels, and LDA values were used to measure the size of

species effects on differential effects. 16S rRNA sequencing results were screened at the genus level using LDA＞4 as the screening criterion (Fig. 5H, I), and microorganisms with higher relative abundance in the group were identified. The results showed that in the control group, *f_Lactobacillaceae*, *o_Lactobacillales*, *g_Ligilactobacillus* dominated; in the model group, *c_Gammaproteobacteria*, *p_Proteobacteria*, *o_Xanthomonadales_616009* dominated; in the TFA group, *c_Bacilli*, *p_Firmicutes_D*, *o_Erysipelotrichales* dominated.

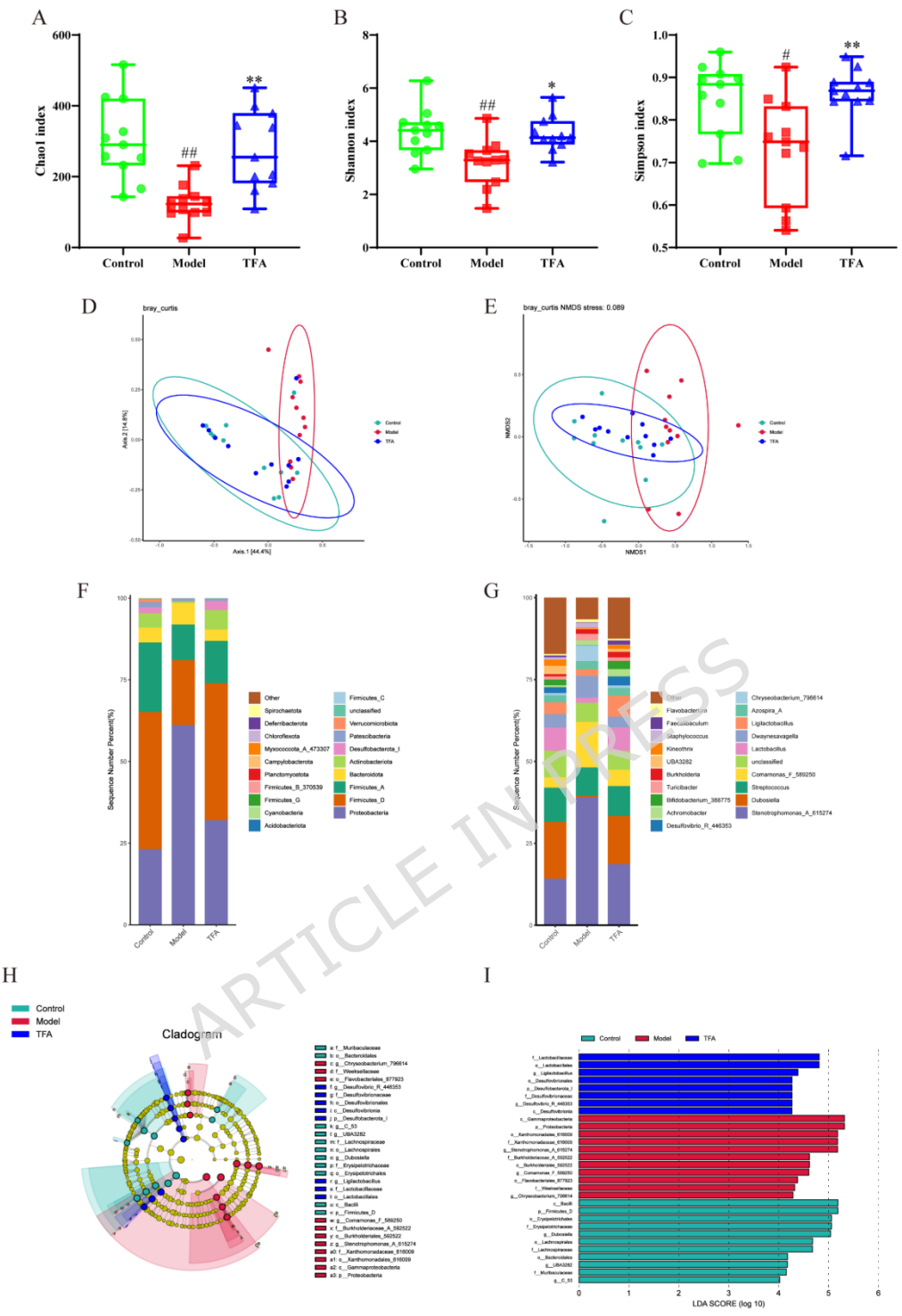

Fig.5. TFA modulated the gut microbiota dysbiosis in mice induced by CCl_4. (A) Alpha diversity Chao1 index. (B) Alpha diversity Shannon index. (C) Alpha diversity Simpson index. (D) PCoA analysis of intestinal microbiota of mice in each group. (E) NMDS analysis of intestinal microbiota in each group. (F) Bar chart of relative abundance of

intestinal microbiota phylum classification level of mice in each group. (G) Bar chart of relative abundance of intestinal microbiota genus classification level of mice in each group. (H) Cladogram of intestinal microbiota in each group. (I) LDA score distribution of intestinal microbiota in each group. Data were expressed as mean±SD (n=10). $^{\#}P<0.05$, $^{\#\#}P<0.01$, vs control group. $^{*}P<0.05$, $^{**}P<0.01$, vs model group.

3.5 Integrated Analysis of Metabolomics and 16S rRNA sequencing of intestinal microbiota

To elucidate the functional interplay between the intestinal microbiota and host metabolism in CCl_4-induced liver fibrosis, we performed an integrated analysis of 16S rRNA sequencing data and serum metabolomics. Spearman correlation analyses were conducted between microbiota (at phylum and genus levels) and key indicators of liver fibrosis (HA, Col-IV) and inflammation (IL-6, TNF-α), with p-values adjusted for multiple comparisons using the Benjamini-Hochberg FDR method. Adjusted p-values<0.05 was considered statistically significant.

As shown in Fig. 6A, pro-inflammatory and profibrotic factors clustered within the fourth quadrant, closely associated with the model group. At the genus level (Fig. 6B, C), *Chryseobacterium_796614*, *Comamonas_F_589250*, and *Stenotrophomonas_A_615274* were significantly positively correlated with disease markers, whereas beneficial genera

including *Akkermansia*, *Adlercreutzia_404257*, *Bifidobacterium_388775*, and *Dubosiella* showed strong negative correlations. Similarly, at the phylum level (Fig. 6D), *Proteobacteria* and *Bacteroidota* abundance correlated positively with disease severity, while *Firmicutes*, *Actinobacteriota*, and *Desulfobacterota* were negatively correlated.

We further examined correlations between serum metabolites and disease indicators (Fig. 6E). Metabolites such as cholestenone, taurocholate, cortisol, and tetrahydrocortisone were positively associated with fibro-inflammatory markers, whereas deoxycytidine, 3-methylhistidine, and phalloidin exhibited negative correlations.

Finally, spearman correlation analysis revealed significant microbiota-metabolite interactions (Fig. 6F). For instance, *Chryseobacterium_796614* correlated positively with L-pyroglutamic acid, D-proline, ornithine, and trigonelline, and negatively with DL-arginine. In contrast, *Clostridium_Q_134526* showed an inverse relationship with these metabolites. These findings suggest that TFA may ameliorate liver fibrosis by restoring beneficial microbiota (*Firmicutes* and *Bifidobacterium*), suppressing pathobionts (*Proteobacteria*), and consequently rectifying dysregulated metabolic pathways.

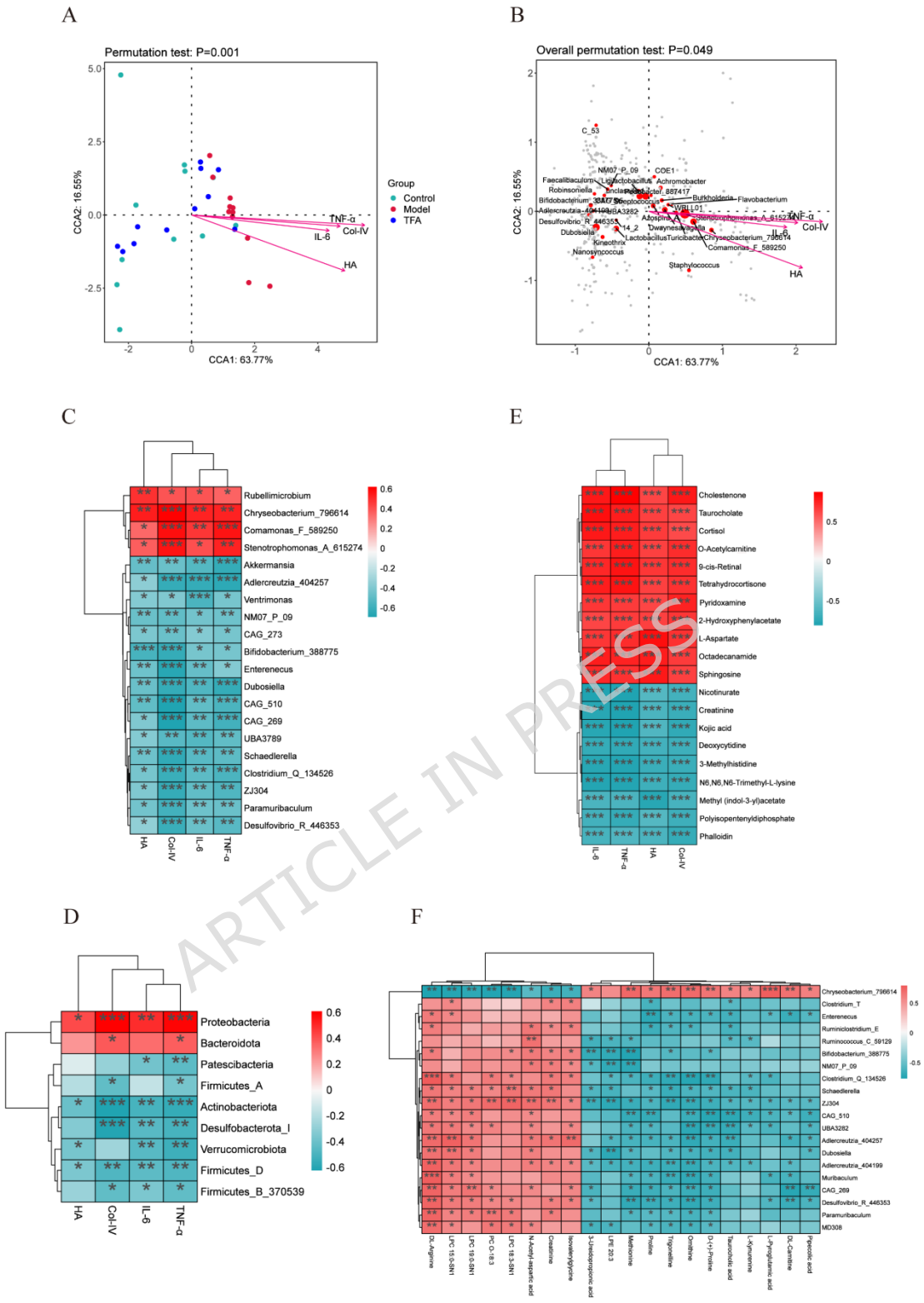

Fig.6. Correlation between metabolites and microbiota composition. (A) Gut microbial composition based on genus level and environmental factors analyzed by mapping tests. (B) Overreplacement test plot of gut microbes based on generic level and environmental

factors. (C) Spearman's rank correlation in the form of a heat map of 20 genera and indicators of liver fibrosis and inflammation. (D) Spearman's rank correlation in the form of a heat map of phylum levels and indicators of liver fibrosis and inflammation. (E) Association of metabolites with liver fibrosis indicators and inflammatory factors based on Spearman correlation analysis. (F) Heat map of the correlation between metabolites and microbiota composition in CCl_4-induced liver fibrosis mice. Red indicates a positive correlation, green indicates a negative correlation, and the intensity of the color represents the strength of the correlation. Only correlations with an FDR-adjusted $p < 0.05$ are displayed. * indicating an FDR-adjusted $p < 0.05$, ** indicating an FDR-adjusted $p < 0.01$, ***indicating an FDR-adjusted $p < 0.001$.

3.6 Validation of key proteins on the arachidonic acid pathway

To validate the involvement of arachidonic acid metabolism in the anti-fibrotic mechanism of TFA, we examined the protein expression of key proteins in this pathway-CYP1A1, CYP2E1, and ALOX1-using immunohistochemistry and western blot analysis.

As shown in Fig. 7A-H, CCl_4-induced liver fibrosis resulted in significant upregulation of CYP1A1, CYP2E1, and ALOX15 compared to the control group ($P < 0.01$). TFA treatment effectively reversed these changes, markedly reducing the expression of all three proteins ($P < 0.05$, 0.01).

Furthermore, western blot analysis of classic fibrosis markers confirmed that TFA administration significantly suppressed the

expression of α-SMA and collagen III (Fig. 7E, I and J), consistent with its anti-fibrotic effects. These results suggest that TFA ameliorates liver fibrosis partly through modulating the arachidonic acid metabolic pathway, specifically by downregulating CYP1A1, CYP2E1, and ALOX15.

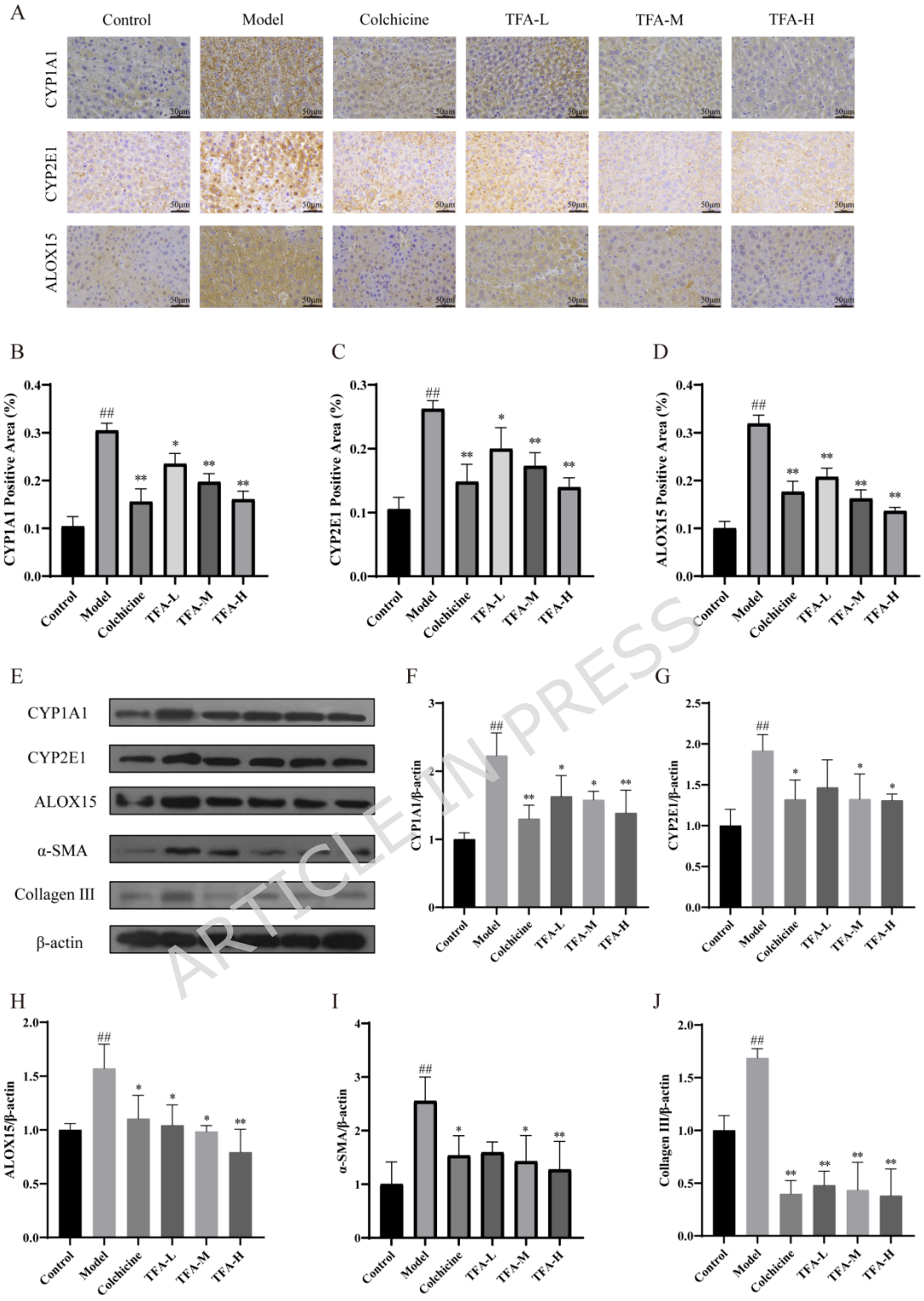

Fig.7. TFA ameliorates liver fibrosis by regulating arachidonic acid metabolism-related proteins and inhibiting HSC activation. (A) Immunohistochemical analysis for CYP1A1, CYP2E1, and ALOX15, 40×, bar=50 μm; (B-D) Semi-quantitative analysis of the protein

expression level of CYP1A1, CYP2E1 and ALOX15; (E) Western bolt analysis for CYP1A1, CYP2E1, ALOX15, α-SMA and Collagen Ⅲ; (F-J) Quantification of band intensity for CYP1A1/β−actin, CYP2E1/β−actin, ALOX15/β−actin, α-SMA/β−actin and Collagen Ⅲ/β−actin ratios.Data were expressed as mean ± SD (n=10). $^{\#\#}P<0.01$, vs control group. $^{*}P<0.05$, $^{**}P<0.01$, vs model group.

4. Discussion

Liver fibrosis is a pathological scarring process driven by chronic liver injury, characterized by excessive deposition of extracellular matrix. In this study, we employed a well-established model of chronic liver fibrosis induced by repeated CCl_4 exposure in mice, which recapitulates key features of human disease—sustained hepatocyte injury, inflammation, and regenerative repair cycles. Using this model, we demonstrated that TFA significantly attenuated CCl_4-induced liver injury, as evidenced by reduced serum ALT and AST levels, decreased oxidative stress (elevated SOD, GSH-Px, and reduced MDA), and lower profibrotic markers (HA and Col-IV). Histological improvements further confirmed the protective effect of TFA.

A key finding is the modulation of arachidonic acid metabolism by TFA. We observed elevated levels of 20-HETE and 16(R)-HETE, metabolites linked to oxidative stress and inflammation via CYP450 and LOX pathways, in fibrotic mice, which were reversed by TFA.

Consistent with prior reports that 20-HETE promotes ROS and activates NF-κB and MAPK/ERK pathways[30], our results suggest TFA may disrupt this pro-fibrotic signaling. Immunohistochemistry and Western blotting further revealed that TFA downregulated hepatic CYP1A1, CYP2E1, and ALOX15, implicating these enzymes as potential targets for TFA in regulating arachidonic acid metabolism. This aligns with, yet mechanistically extends, previous studies on TFA's hepatoprotection in acute and cholestatic models[10], by highlighting its role in chronic fibrosis through metabolic reprogramming.

Recent studies have found that the liver and the intestine can interact with each other through various physiological activities[33]. When the ecological balance of intestinal microbiota is broken, dysbiosis occurs, and the intestinal barrier is damaged, pathogenic bacteria and metabolites will seep out of the intestinal lumen and enter the liver, thus threatening the health of the host; when chronic liver disease occurs there are significant differences in the intestinal microbiota due to abnormal secretion of bile acids and slowing of intestinal peristalsis[34], so there is a correlation between changes in the intestinal microbiota and liver fibrosis. Therefore, our study underscores the role of gut-liver axis in TFA's mechanism. CCl_4 induction disturbed gut microbiota composition,

TFA treatment restored microbial richness and community structure, increased beneficial taxa (*Firmicutes*, *Actinobacteriota*), and suppressed conditionally pathogenic bacteria (*Proteobacteria*). These changes likely contribute to reduced systemic inflammation and enhanced intestinal barrier function, thereby alleviating liver injury through the gut-liver axis. This is consistent with growing evidence that flavonoid-rich extracts ameliorate metabolic and inflammatory disorders via microbiota modulation[35, 36].

The integrated analysis of metabolomic and microbiota data provides compelling, albeit correlative, evidence that TFA's anti-fibrotic effects are mediated through multi-level modulation of the gut-liver axis. Integrative analysis revealed significant associations between specific bacterial genera (e.g., *Chryseobacterium*, *Comamonas*) and fibro-inflammatory markers, as well as between microbiota shifts and altered metabolic pathways such as glycerophospholipid and tryptophan metabolism. These correlations suggest potential mechanistic links: for instance, the enrichment of *Bifidobacterium* and *Dubosiella* may contribute to the observed recovery in glycerophospholipid and energy metabolism, as short-chain fatty acids enhance intestinal integrity and reduce hepatic inflammation[37, 38]. Conversely, the reduction in *Proteobacteria*, a phylum often associated with endotoxin

production, may underlie the decrease in inflammatory mediators (TNF-α, IL-6) and arachidonic acid metabolites such as 20-HETE, which promote oxidative stress and fibrogenesis. The negative correlation between *Akkermansia* and fibro-inflammatory markers further supports a model in which TFA fosters a microbiota environment conducive to metabolic homeostasis and reduced inflammation[39, 40]. Although our data do not establish causality, they collectively suggest a systems-level mechanism whereby TFA rectifies gut ecological imbalance and host metabolic dysregulation, thereby mitigating liver fibrosis. Future studies using germ-free models or fecal microbiota transplantation could further validate these mechanistic interactions.

Several limitations should be acknowledged. First, this study was conducted only in male mice. Given recognized sex differences in immune response, fibrosis progression, and gut microbiota composition, future studies should include female animals to evaluate potential sex-dimorphic effects. Second, the CCl_4 model, while reproducible and widely used, represents an accelerated form of fibrosis. Translational extrapolation to human chronic liver diseases requires caution and further validation in clinical settings or additional models.

In conclusion, TFA alleviates liver fibrosis not only through classical antioxidant and anti-inflammatory pathways but also via multi-scale regulation of host metabolism and intestinal microbiota. Our findings underscore the therapeutic potential of TFA as a multi-target agent acting on the gut-liver-metabolism axis and provide a rationale for further investigation into its use in chronic liver diseases.

Conclusion

In this preclinical study, we demonstrated that TFA ameliorated oxidative stress and inflammation in CCl_4-induced mice model of liver fibrosis, thereby alleviating liver injury. The anti-fibrotic effects of TFA were associated with modulation of intestinal microbiota composition and serum metabolite profiles. Specifically, TFA treatment increased microbial diversity and beneficial bacteria, reduced conditional pathogens, and regulated key metabolic pathways—including arachidonic acid metabolism. These results suggest that TFA may hold potential as a multi-target agent for alleviating liver fibrosis, though further studies are required to validate these mechanisms and assess translational relevance in humans.

Declarations

Ethics approval and consent to participate

This study was approved by the Animal Ethics Committee of Suzhong Pharmaceutical Group Co., Ltd. (Approval Code: SZSW-2023082401). All methods are reported in accordance with ARRIVE guidelines.

Author contributions

Dengya Li drafted the manuscript. Emily Heya Tang performed the data processing. Yan Zhang, Shuying Song and Luwan Xing performed Western blot experiments and conducted data analysis. Haitao Ge and Fujiang Wang critically appraised the paper and gave final suggestions. All authors contributed to the final approval of the manuscript.

Competing interests

The authors declare that they have no competing interests.

Funding

This research did not receive any specific grant from any funding agency in the public, commercial or not-for-profit sector.

Availability of data and materials

The data reported in this paper have been deposited in the OMIX, China National Center for Bioinformation / Beijing Institute of Genomics, Chinese Academy of Sciences

(https://ngdc.cncb.ac.cn/omix: accession no.OMIX010404 and accession no.OMIX010405).

Consent for publication

Not applicable.

Acknowledgement

Sequencing service and data analysis service were provided by Wekemo Tech Group Co., Ltd. Shenzhen China.

Reference

[1] M.M. Aydin, K.C. Akcali, Liver fibrosis, Turk J Gastroenterol, 29 (2018) 14-21.
[2] T. Higashi, S.L. Friedman, Y. Hoshida, Hepatic stellate cells as key target in liver fibrosis, Adv Drug Deliv Rev, 121 (2017) 27-42.
[3] M. Pinzani, Pathophysiology of Liver Fibrosis, Dig Dis, 33 (2015) 492-497.
[4] S. Nafees, S. Rashid, N. Ali, et al., Rutin ameliorates cyclophosphamide induced oxidative stress and inflammation in Wistar rats: role of NFkappaB/MAPK pathway, Chem Biol Interact, 231 (2015) 98-107.
[5] Y.K. Jung, H.J. Yim, Reversal of liver cirrhosis: current evidence and expectations, Korean J Intern Med, 32 (2017) 213-228.
[6] N.P. Commission, Pharmacopoeia of the People's Republic of China, China Medical Science Press, Beijing, 2020.
[7] L. Zhang, P. Li, C.Y. Xing, et al., Efficacy and safety of Abelmoschus manihot for primary glomerular disease: a prospective, multicenter randomized controlled clinical trial, Am J Kidney Dis, 64 (2014) 57-65.
[8] A. Trendafilova, M. Todorova, M. Nikolova, et al., Flavonoid constituents and free radical scavenging activity of Alchemilla mollis, Nat Prod Commun, 6 (2011) 1851-1854.
[9] N. Li, H. Tang, L. Wu, et al., Chemical constituents, clinical efficacy and molecular mechanisms of the ethanol extract of Abelmoschus manihot flowers in treatment of kidney diseases, Phytother Res, 35 (2021) 198-206.
[10] J.Y. Yan, G. Ai, X.J. Zhang, et al., Investigations of the total flavonoids extracted from flowers of Abelmoschus manihot (L.) Medic against alpha-naphthylisothiocyanate-induced cholestatic liver injury in rats, J Ethnopharmacol, 172 (2015) 202-213.
[11] Y. Wei, J. Li, B. Zhu, et al., Metagenomic comparison of intestinal microbiota between normal and liver fibrotic rhesus macaques (Macaca mulatta), Sci Rep, 14 (2024) 15677.
[12] Y. Fan, Y. Dong, Z. Gai, et al., Lactiplantibacillus plantarum Lp05 protects against ethanol-induced liver injury in zebrafish through metabolic and microbiota modulation, Sci Rep, 15 (2025) 22584.
[13] A.J. Glenwright, K.R. Pothula, S.P. Bhamidimarri, et al., Structural basis for nutrient acquisition by dominant members of the human gut microbiota, Nature, 541 (2017) 407-411.
[14] J.L. Sonnenburg, F. Backhed, Diet-microbiota interactions as moderators of human metabolism, Nature, 535 (2016) 56-64.

[15] N. Geva-Zatorsky, E. Sefik, L. Kua, et al., Mining the Human Gut Microbiota for Immunomodulatory Organisms, Cell, 168 (2017) 928-943 e911.
[16] X. Wang, A. Zhang, H. Sun, Power of metabolomics in diagnosis and biomarker discovery of hepatocellular carcinoma, Hepatology, 57 (2013) 2072-2077.
[17] Y. Zhang, M. Zhang, H. Li, et al., Serum metabonomics study of the hepatoprotective effect of amarogentin on CCl(4)-induced liver fibrosis in mice by GC-TOF-MS analysis, J Pharm Biomed Anal, 149 (2018) 120-127.
[18] D.S. Wishart, Emerging applications of metabolomics in drug discovery and precision medicine, Nat Rev Drug Discov, 15 (2016) 473-484.
[19] J. Han, J. Meng, S. Chen, et al., Integrative analysis of the gut microbiota and metabolome in rats treated with rice straw biochar by 16S rRNA gene sequencing and LC/MS-based metabolomics, Sci Rep, 9 (2019) 17860.
[20] Y. Hu, X. Ni, Q. Chen, et al., Predicting diabetic kidney disease with serum metabolomics and gut microbiota, Sci Rep, 15 (2025) 12179.
[21] S.C. Yanguas, B. Cogliati, J. Willebrords, et al., Experimental models of liver fibrosis, Arch Toxicol, 90 (2016) 1025-1048.
[22] E.J. Want, G. O'Maille, C.A. Smith, et al., Solvent-dependent metabolite distribution, clustering, and protein extraction for serum profiling with mass spectrometry, Anal Chem, 78 (2006) 743-752.
[23] T. Barri, L.O. Dragsted, UPLC-ESI-QTOF/MS and multivariate data analysis for blood plasma and serum metabolomics: effect of experimental artefacts and anticoagulant, Anal Chim Acta, 768 (2013) 118-128.
[24] M. Kanehisa, M. Furumichi, M. Tanabe, et al., KEGG: new perspectives on genomes, pathways, diseases and drugs, Nucleic Acids Res, 45 (2017) D353-D361.
[25] M. Kanehisa, M. Furumichi, Y. Sato, et al., KEGG for taxonomy-based analysis of pathways and genomes, Nucleic Acids Res, 51 (2023) D587-D592.
[26] B.J. Callahan, P.J. McMurdie, M.J. Rosen, et al., DADA2: High-resolution sample inference from Illumina amplicon data, Nat Methods, 13 (2016) 581-583.
[27] B.J. Callahan, P.J. McMurdie, S.P. Holmes, Exact sequence variants should replace operational taxonomic units in marker-gene data analysis, ISME J, 11 (2017) 2639-2643.

[28] J.T. Nearing, G.M. Douglas, M.G. Hayes, et al., Microbiome differential abundance methods produce different results across 38 datasets, Nat Commun, 13 (2022) 342.
[29] R.C. Edgar, Updating the 97% identity threshold for 16S ribosomal RNA OTUs, Bioinformatics, 34 (2018) 2371-2375.
[30] T. Ishizuka, J. Cheng, H. Singh, et al., 20-Hydroxyeicosatetraenoic acid stimulates nuclear factor-kappaB activation and the production of inflammatory cytokines in human endothelial cells, J Pharmacol Exp Ther, 324 (2008) 103-110.
[31] G. Quintas, T. Martinez-Sena, I. Conde, et al., Metabolomic analysis to discriminate drug-induced liver injury (DILI) phenotypes, Arch Toxicol, 95 (2021) 3049-3062.
[32] Y. Mao, Z. Xie, X. Zhang, et al., Ergothioneine Ameliorates Liver Fibrosis by Inhibiting Glycerophospholipids Metabolism and TGF-beta/Smads Signaling Pathway: Based on Metabonomics and Network Pharmacology, J Appl Toxicol, 45 (2025) 514-530.
[33] S. Wan, Y. Nie, Y. Zhang, et al., Gut Microbial Dysbiosis Is Associated With Profibrotic Factors in Liver Fibrosis Mice, Front Cell Infect Microbiol, 10 (2020) 18.
[34] G. Lee, H.J. You, J.S. Bajaj, et al., Distinct signatures of gut microbiome and metabolites associated with significant fibrosis in non-obese NAFLD, Nat Commun, 11 (2020) 4982.
[35] Y. Hu, J. Tang, Y. Xie, et al., Gegen Qinlian decoction ameliorates TNBS-induced ulcerative colitis by regulating Th2/Th1 and Tregs/Th17 cells balance, inhibiting NLRP3 inflammasome activation and reshaping gut microbiota, J Ethnopharmacol, 328 (2024) 117956.
[36] Z. Wang, X. Ren, Z. Peng, et al., Flavonoid-rich extracts of Nelumbo nucifera leaves alleviate obesity in HFD-fed mice via microbiota-dependent modulation of brown fat thermogenesis, J Ethnopharmacol, 354 (2025) 120513.
[37] G. den Besten, K. van Eunen, A.K. Groen, et al., The role of short-chain fatty acids in the interplay between diet, gut microbiota, and host energy metabolism, J Lipid Res, 54 (2013) 2325-2340.
[38] M.G. Tang, L.G. Xiong, J.A. Huang, et al., Theaflavin-3,3'-digallate prevents alcoholic liver injury by suppressing hepatic TLR4/NF-kappaB signaling and modulating the gut-liver axis in mice, J Nutr Biochem, 145 (2025) 110031.
[39] Y. He, Z. Song, Y. Ji, et al., Preventive Effects of l-Glutamine on High-Fat Diet-Induced Metabolic Disorders Linking with Regulation of Intestinal Barrier Integrity, Hepatic Lipid Metabolism, and Gut Microbiota in Rats, J Agric Food Chem, 70 (2022) 11923-11934.

[40] E. Aja, A. Zeng, W. Gray, et al., Health Effects and Therapeutic Potential of the Gut Microbe Akkermansia muciniphila, Nutrients, 17 (2025).

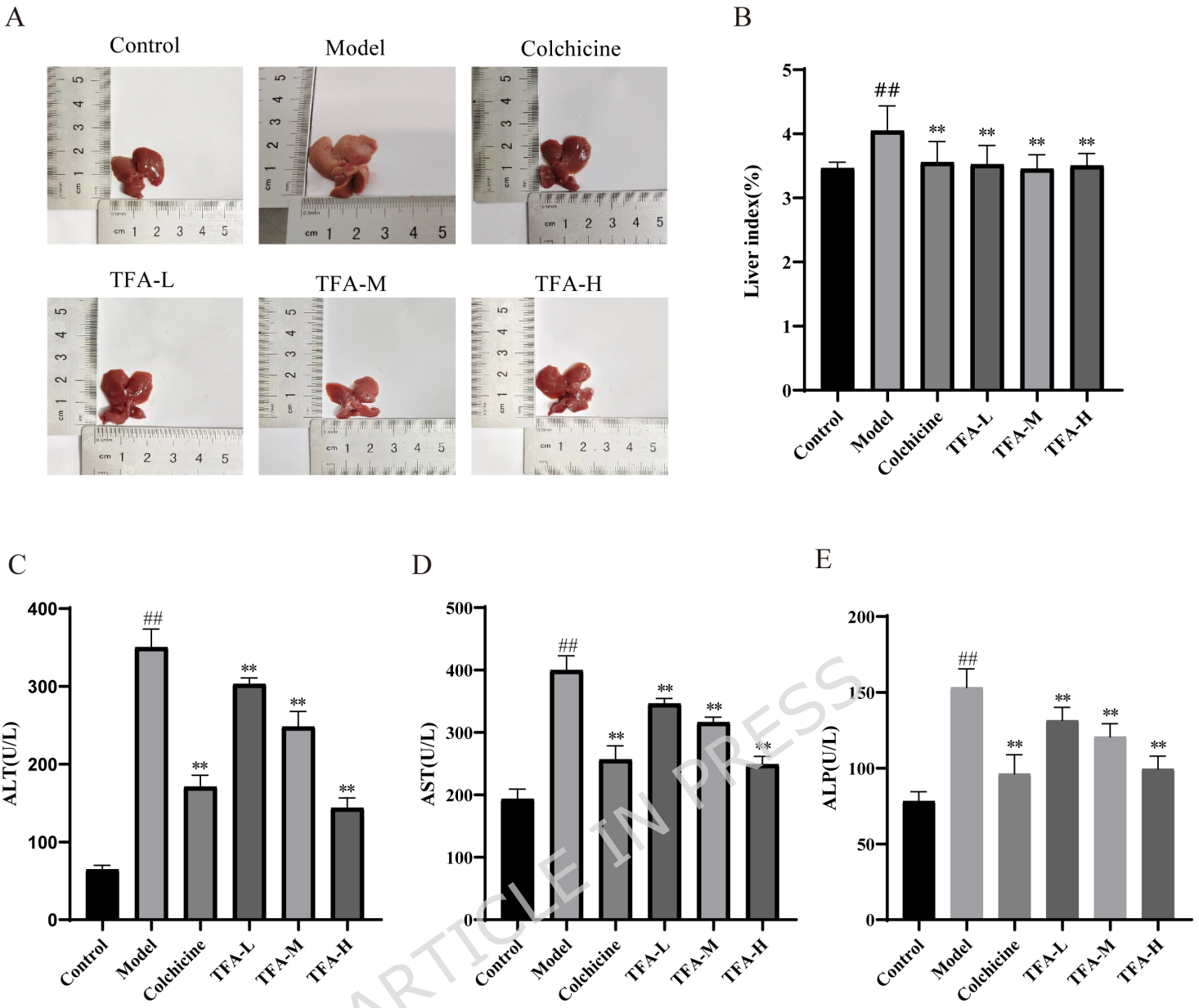

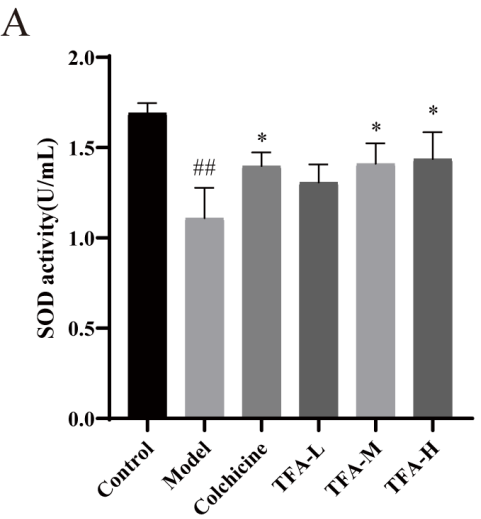

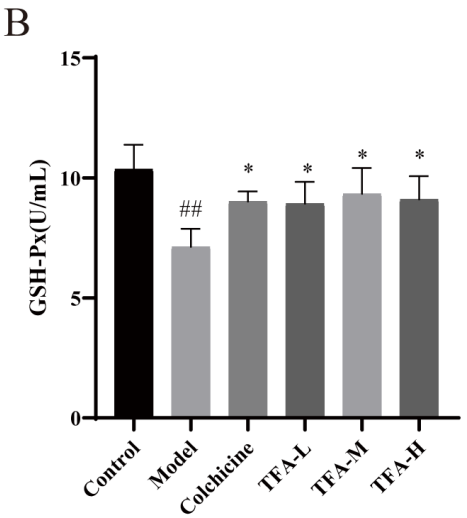

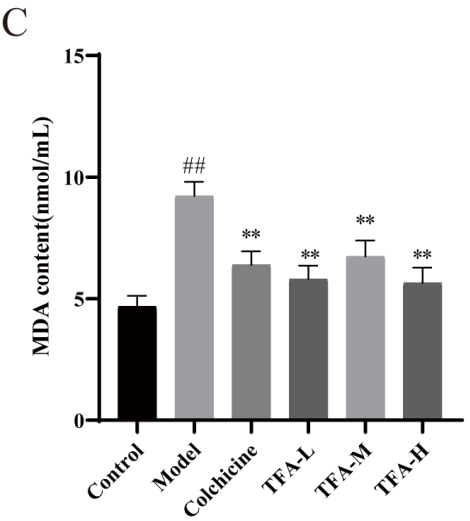

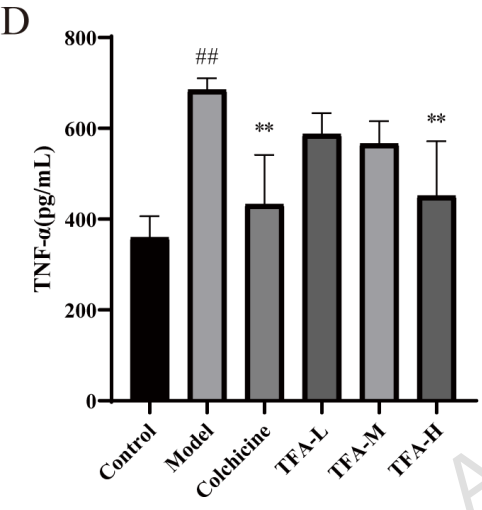

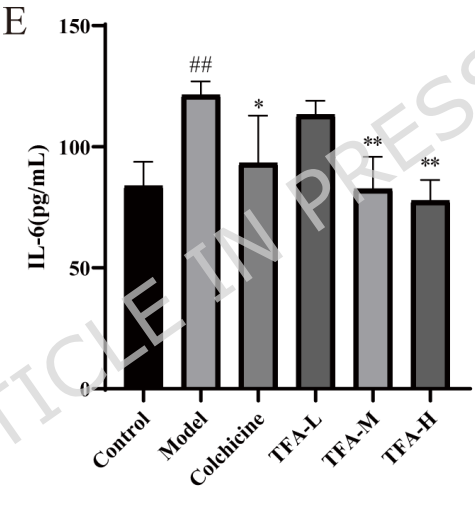

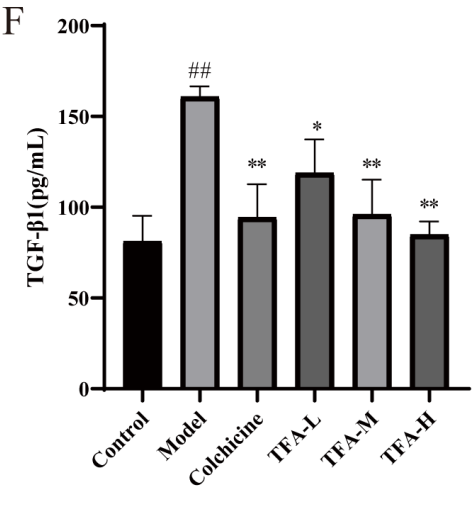

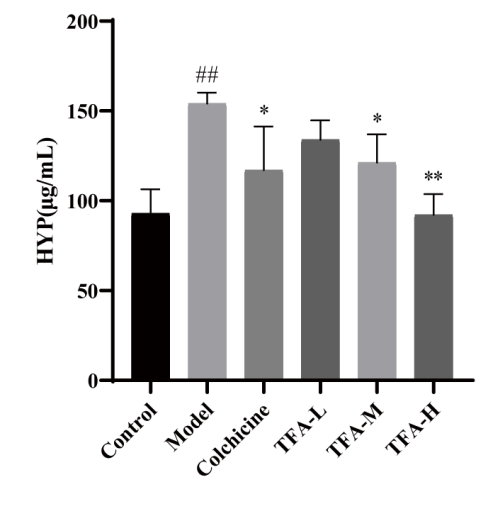

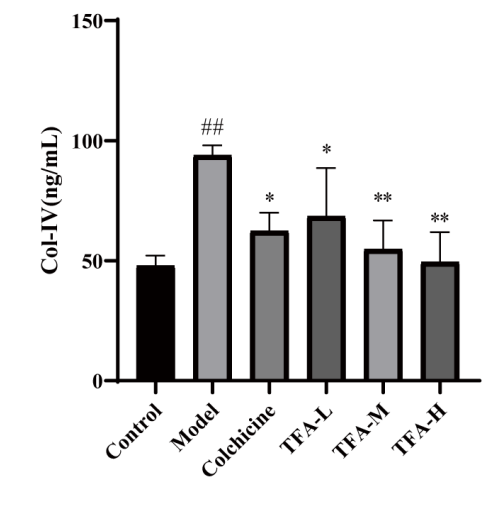

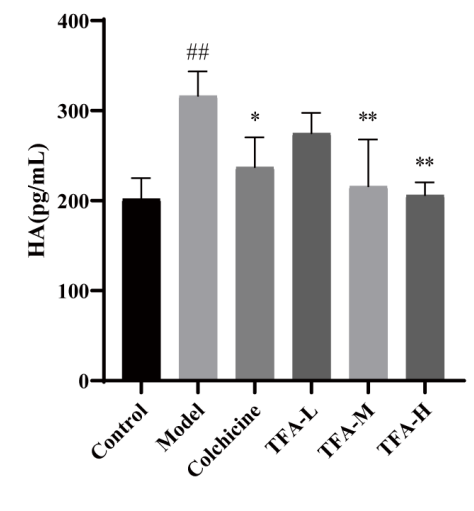

A

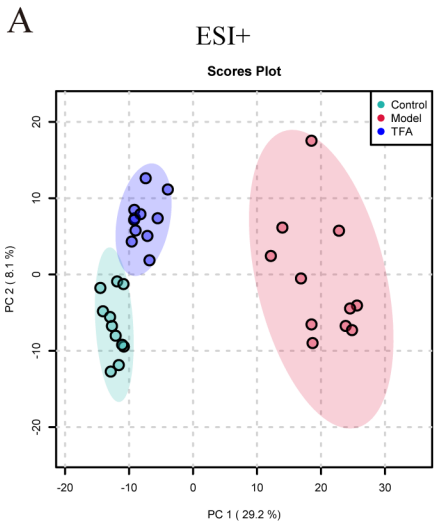

B

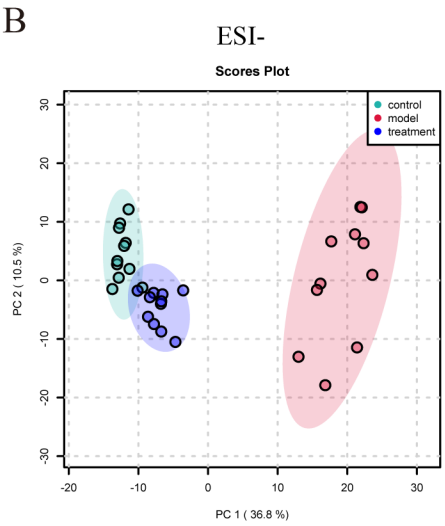

G

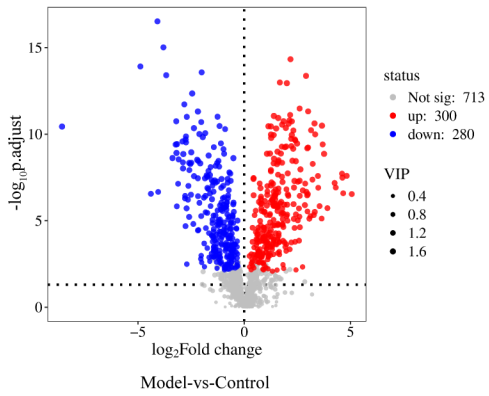

C

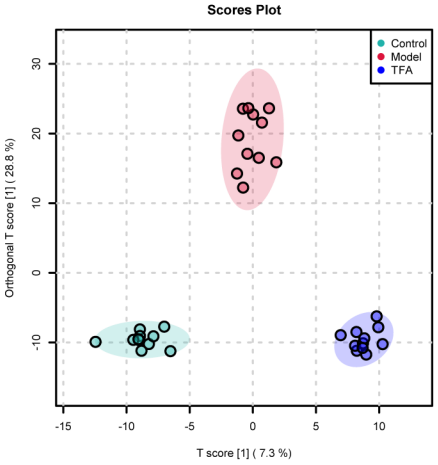

D

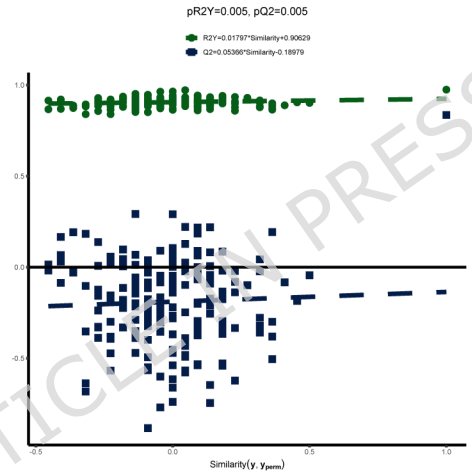

H

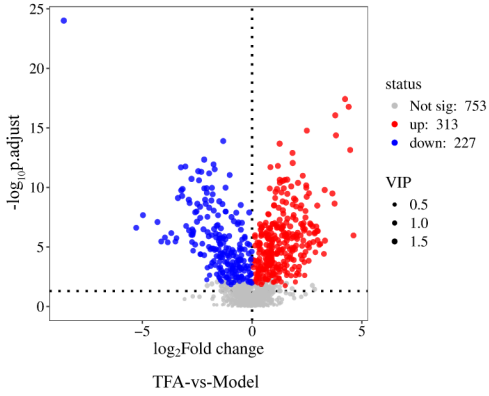

E

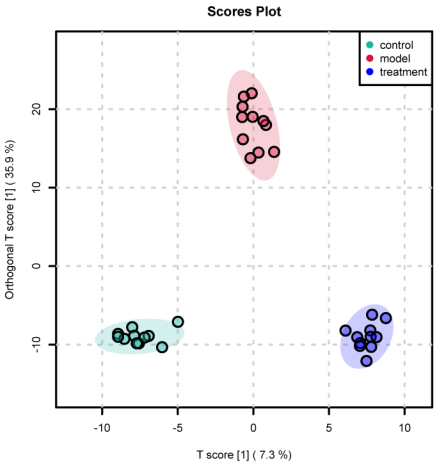

F

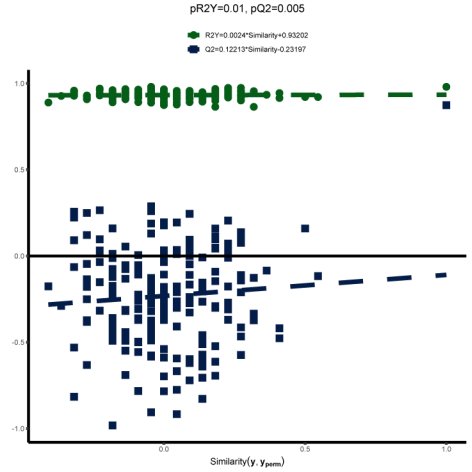

I

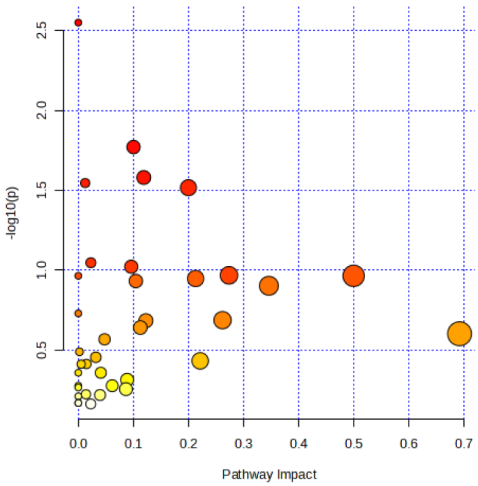

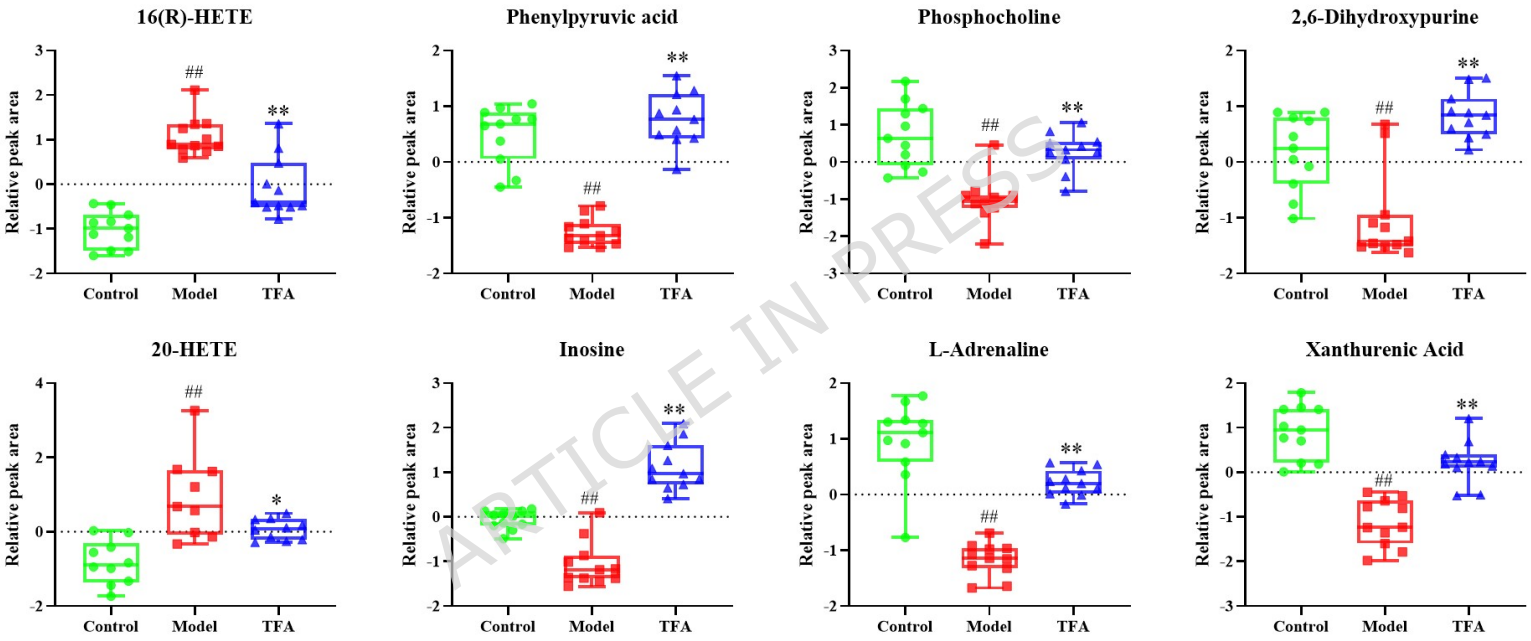

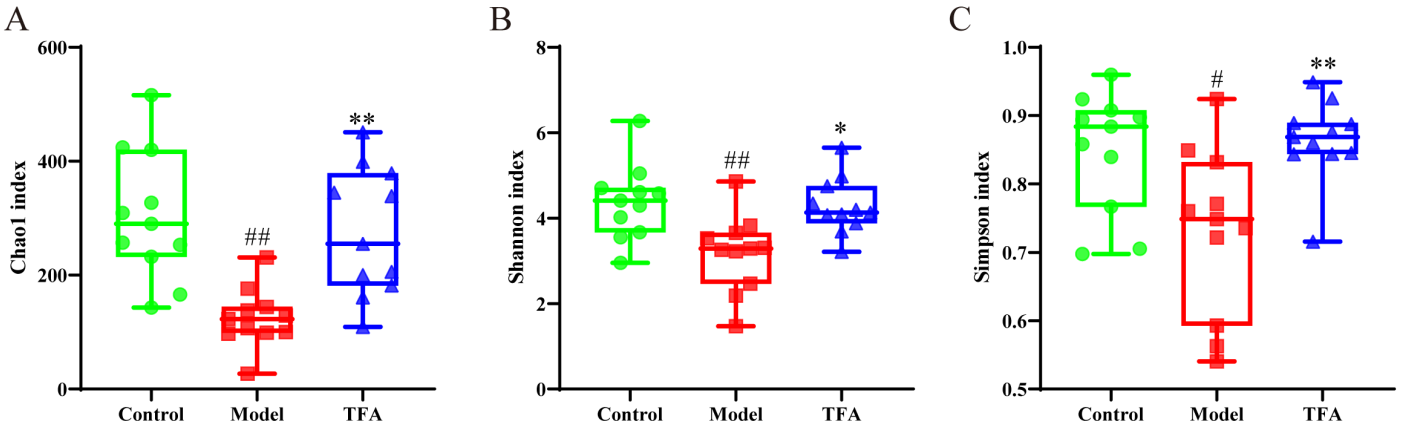

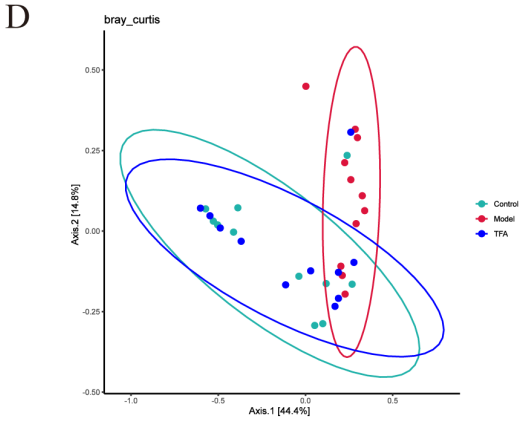

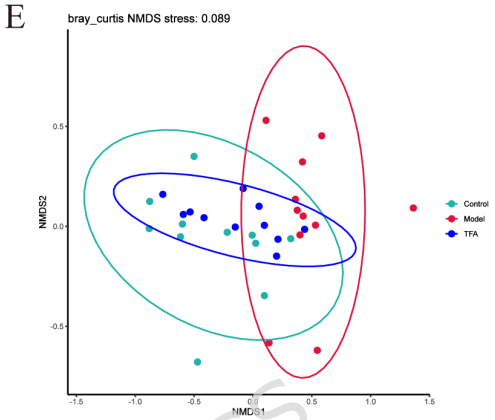

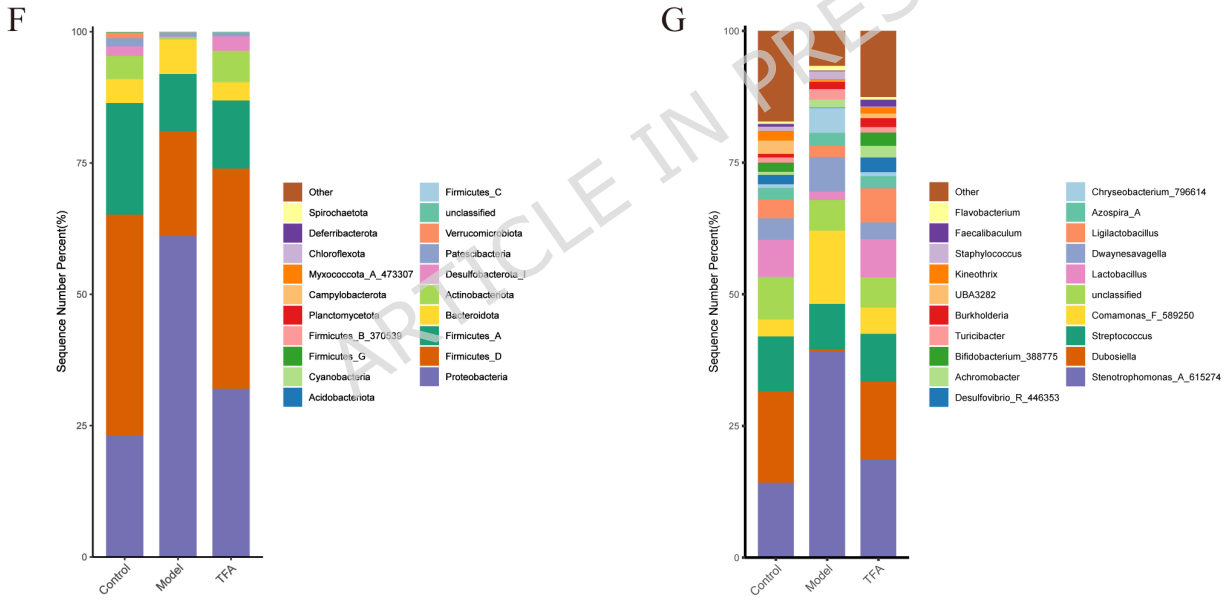

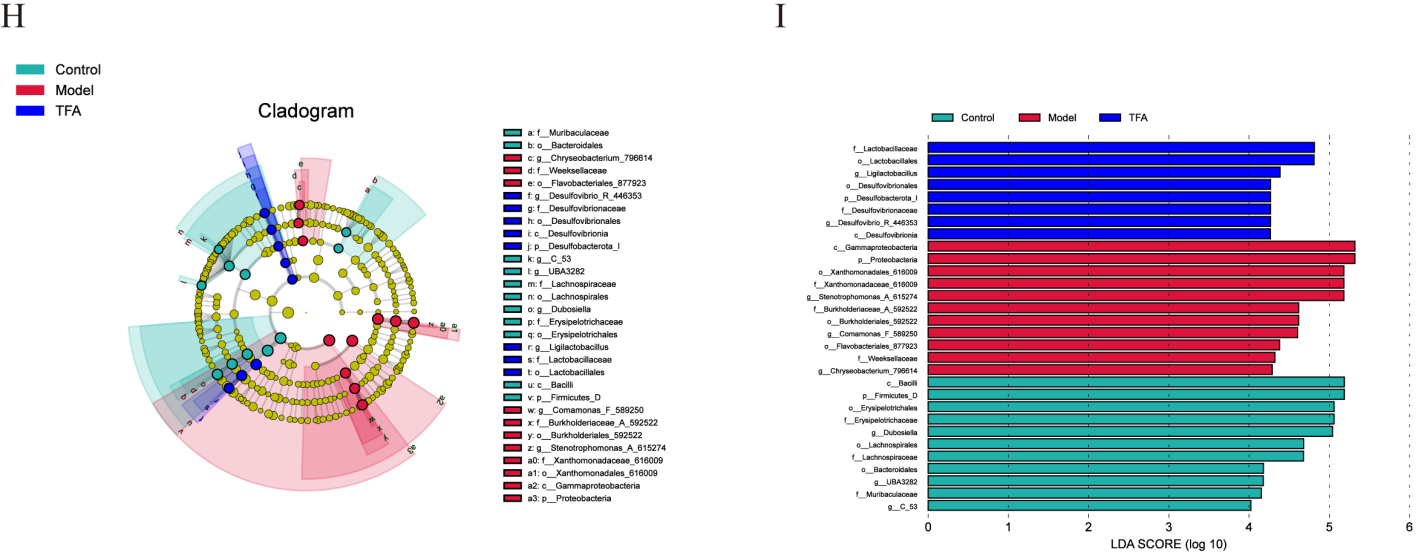

A

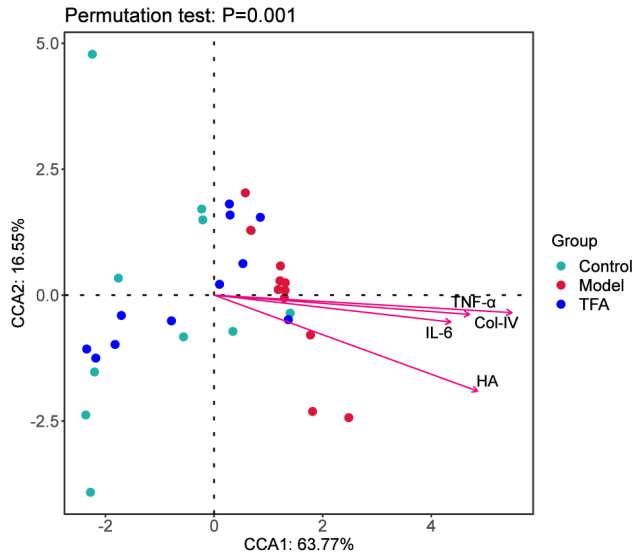

B

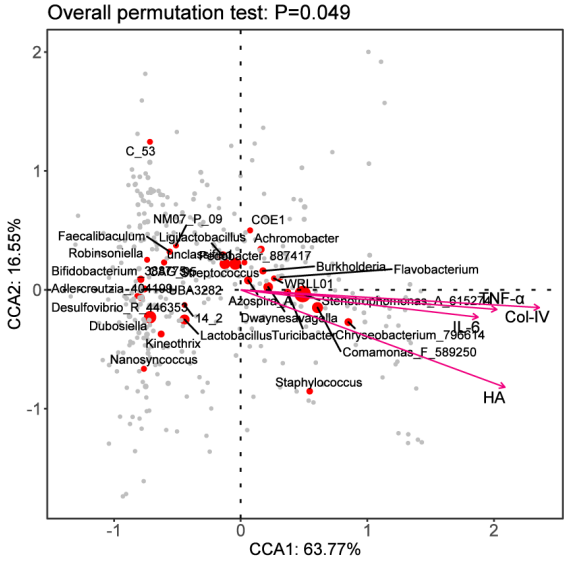

C

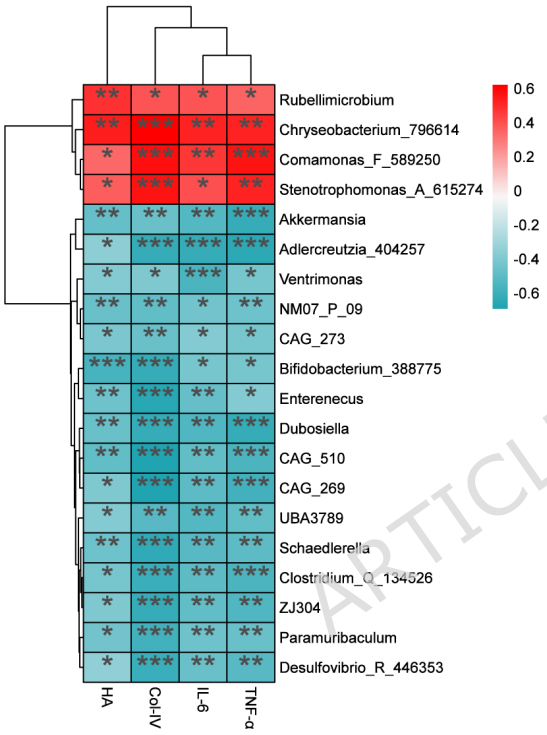

E

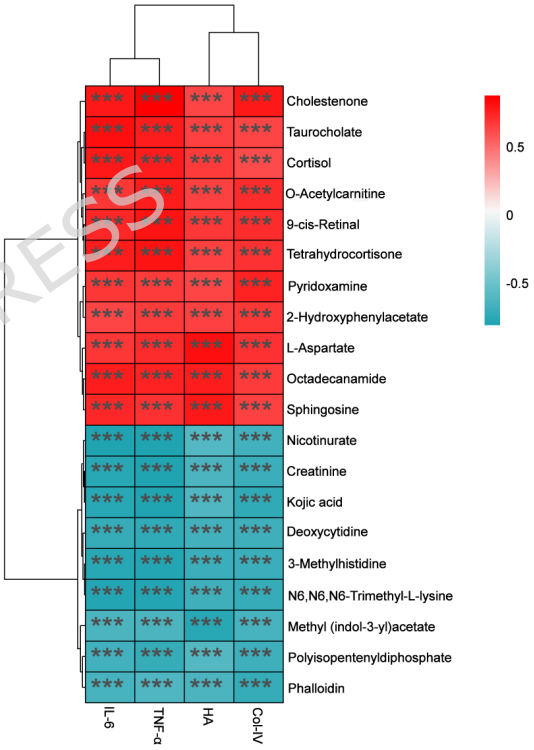

D

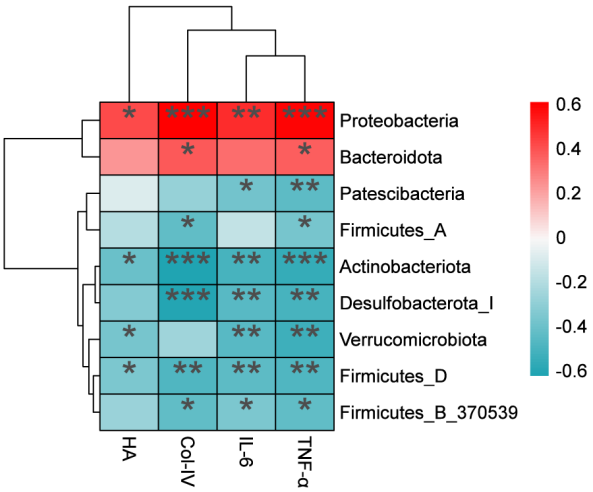

F